APL Materials

Defect modeling in skyrmionic ferromagnetic systems

Cite as: APL Mater. **10**, 010702 (2022); https://doi.org/10.1063/5.0072709
Submitted: 24 September 2021 • Accepted: 16 December 2021 • Published Online: 13 January 2022

Nuria Del-Valle, Josep Castell-Queralt, Leonardo González-Gómez, et al.

Defect modeling in skyrmionic ferromagnetic systems

Cite as: APL Mater. 10, 010702 (2022); doi: 10.1063/5.0072709
Submitted: 24 September 2021 • Accepted: 16 December 2021 •
Published Online: 13 January 2022

Nuria Del-Valle, Josep Castell-Queralt, Leonardo González-Gómez, and Carles Navau[a)]

AFFILIATIONS

Departament de Física, Universitat Autònoma de Barcelona, 08193 Bellaterra, Barcelona, Spain

[a)]Author to whom correspondence should be addressed: carles.navau@uab.cat

ABSTRACT

Defects are unavoidable in real materials. Defects, either intrinsic or artificially incorporated, can alter the material properties. In the particular case of skyrmionic ferromagnetic materials, defects modify the stability and dynamics of the skyrmions. These magnetic structures have aroused great interest due to their potential as information carriers. Hence, the knowledge and control of the influence of defects on skyrmions are essential for their use in applications, such as magnetic memories or information mobility. Aiming to give an overview on defect simulations, we review the most relevant approaches to simulate defects in ferromagnetic materials, hosting skyrmions depending on their size, nature, strength, and quantity.

I. INTRODUCTION

Magnetic skyrmions[1,2] are whirling magnetic structures with nanometric size, high mobility,[3–6] and topological protection.[7,8] These magnetic structures can appear in single crystals of magnetic compounds with a non-centrosymmetric lattice[9] due to the existence of a chiral interaction. This interaction, named Dzyaloshinskii–Moriya (DM) interaction, is induced by spin–orbit coupling in the absence of inversion symmetry in the crystal lattice (bulk DM interaction). Skyrmions are also observed in ultrathin magnetic films epitaxially grown on top of heavy-metal substrates which are subject to large DM interaction. In this case, the interaction is induced at the interface (interfacial DM interaction)[10–12] by the breaking of inversion symmetry due to the strong spin–orbit coupling of the neighboring heavy metal. In multilayers of alternate ferromagnets and heavy metals which interact with each other via a similar mechanism, skyrmions have also been stabilized.[13,14] The conjunction of certain properties, such as small size, high movement capacity, and high stability, makes skyrmions potentially attractive for storing and transporting information based on the one-skyrmion one-bit principle.[6,11,12,15,16] In both cases, individual skyrmion control is a key element in their viability. One of the factors affecting such control is the presence of defects in the host magnetic material. To a greater or lesser extent, defects are present in all real materials. In the case of magnetic materials where skyrmions are formed, defects or impurities influence both stability (statics) and motion (dynamics) of these magnetic textures, which we will review in this Research Update. Therefore, the use of skyrmions in ultradense magnetic memories and logic devices requires an understanding of their interaction with defects.

Theoretical simulations, whether analytical or numerical, are useful tools to deepen the understanding in the field of study. They can explain phenomena already found experimentally and predict the appearance of new ones. In the field of skyrmionic magnetic materials, there are numerous theoretical studies at different scales. These works range from the most fundamental level at the atomic scale, where the magnetic interaction between atoms is studied by first-principles, to the macroscopic scale, where the relevant parameters are the averages of the fundamental interactions. In the particular case of the simulation of defects in the host magnetic material, a large variety of works can be found. Here, we present a review which aims at giving a complete overview of the different ways to simulate defects in skyrmionic magnetic materials and the effects they have on skyrmions. To facilitate the reading and understanding of this Research Update, it has been divided into three blocks depending on the size, range of action, and abundance of the defect. Each block includes the theoretical framework in which the simulation of the different defects is developed and, with the help of

the most representative and relevant theoretical works, the methods used to consider these defects and their influence on the skyrmions. The first block is presented in Sec. II, where different ways to simulate the interaction of skyrmions with atomic defects are studied. The second block is discussed in Sec. III, where defects are no longer atomic and become larger, allowing for the use of the micromagnetic framework and the rigid model to describe the magnetic material. In Sec. IV we find the third block in which systems with a large number of intrinsic defects giving the material a certain degree of granularity and disorder are analyzed. Finally, some concluding remarks and a summary table are presented in Sec. V.

II. DEFECTS AS ATOMS

From a classical point of view, a magnetic material can be considered as a collection of atoms/ions on a regular lattice. Each atom/ion is magnetically represented by a localized magnetic moment whose modulus (a non-integer number of Bohr magnetons) corresponds to the total spin of all electrons bound to the atom/ion. In energy terms, this translates into the Effective Hamiltonian or atomistic Extended Heisenberg Hamiltonian (EHH), which is expressed by

$$\mathscr{H} = -\frac{1}{2}\sum_i \sum_{j=i*} J_{ij}\, \hat{s}_i \cdot \hat{s}_j - \frac{1}{2}\sum_i \sum_{j=i*} \mathbf{d}_{ij} \cdot (\hat{s}_i \times \hat{s}_j) - \sum_i k_i (\hat{u}_k \cdot \hat{s}_i)^2 - \mu_0 \sum_i \mathbf{S}_i \cdot \mathbf{H}_a - \frac{1}{2}\mu_0 \sum_i \sum_{j \neq i} \mathbf{S}_i \cdot \mathbf{H}_j^{(i)}, \quad (1)$$

where the unit vector $\hat{s}_i = \mathbf{S}_i/S_i$ defines the direction of the magnetic moment $\mathbf{S}_i$ at site i and $j = i^*$ means that the summation is carried over the j-magnetic moments that are first neighbors of i. The first term describes the Heisenberg exchange interaction, with J_{ij} being the exchange integrals. The second term corresponds to the DM interaction, with $\mathbf{d}_{ij}$ being the DM vectors. In the case of bulk DM interaction, $\mathbf{d}_{ij} = d_{ij}\hat{u}_{ij}$, $\hat{u}_{ij}$ being the unit vector connecting $\mathbf{S}_i$ and $\mathbf{S}_j$, and in the case of interfacial DM interaction, $\mathbf{d}_{ij} = d_{ij}(\hat{u}_{ij} \times \hat{z})$, with $\hat{z}$ being normal to the interface. The third term is related to the magnetocrystalline anisotropy energy. Although different anisotropy types exist,[17,18] throughout this Research Update, we will only consider the uniaxial case as it is the most commonly used in theoretical studies. Here, k_i describes the uniaxial anisotropy energy with $\hat{u}_k$ as the easy axis. Usually, in a homogeneous and isotropic defect-free sample, the magnitudes of J_{ij}, d_{ij}, and k_i are considered as the constants J, d, and k, respectively. The fourth term is the Zeeman contribution due to an external applied magnetic field $\mathbf{H}_a$, and the last term corresponds to the magnetostatic or dipole–dipole interaction where $\mathbf{H}_j^{(i)}$ is the magnetic dipolar field created by the jth magnetic moment over the ith one. In thin film samples, this last term can be renormalized inside an effective anisotropy factor, reducing the k factor.[19–21]

Within the atomistic framework, we find two ways of considering atomic defects. On the one hand, defects can be simulated by directly modifying the atomic structure of the material, for example, by replacing[22] or adding[23,24] few atoms [see Fig. 1(a)]. On the other hand, defects can also be implemented by

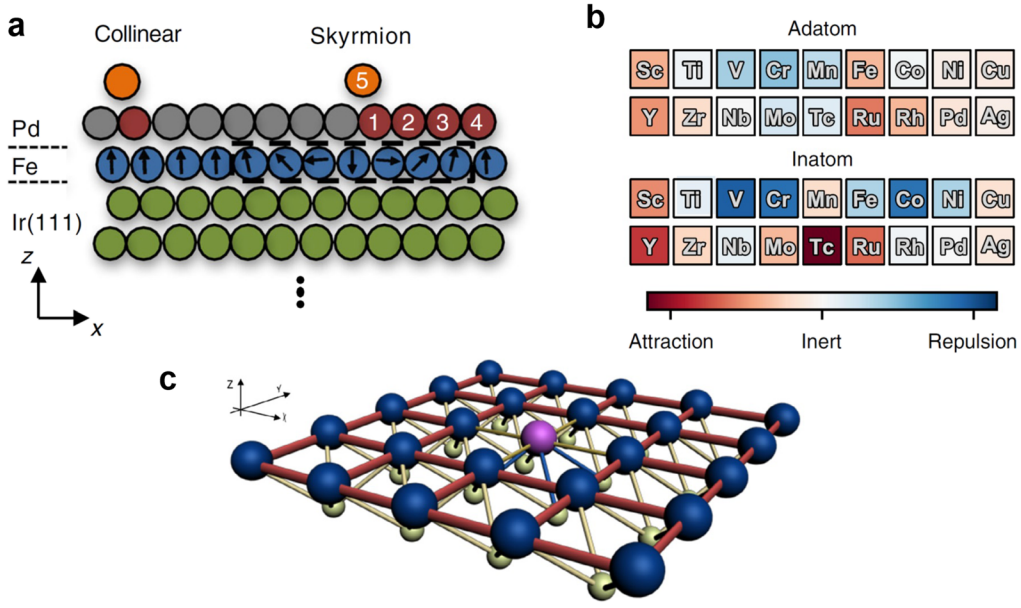

FIG. 1. Sketches of the different kinds of atomic defects. (a) Cross section of the PdFe/Ir(111) surface with inatom and adatom defects (positions: labels 1–5) with the Periodic Table in (b). The color scale indicates the strength of the binding energies. Red corresponds to attraction, and blue corresponds to repulsion. (a) and (b) are reproduced with permission from Lima Fernandes *et al.*, Nat. Commun. **9**, 4395 (2018). Copyright 2018 Author(s), licensed under a Creative Commons Attribution (CC BY) license. (c) A defect (central lighter position) in an array of atoms with different interfacial DM interactions (blue links with the bottom layer) and different exchange interactions (in-plane yellow links). In the rest of the sample, the red and yellow links symbolize the exchange and DM interactions, respectively [reproduced with permission from Navau *et al.*, J. Magn. Magn. Mater. **465**, 709 (2018). Copyright 2018, Elsevier B. V.].

locally modifying the interactions between neighboring magnetic moments by altering either the constants J, d, k[25,26] [see Fig. 1(c)] or themselves.[27]

Choi *et al.*[22] explained an example of the first type of defect simulation. They studied how the pinning energy of a skyrmion in MnSi is modified (attraction or repulsion) when one site of Mn is substituted by Zn, Ir, or Co atomic impurities and one site of Si is replaced by a Pb atom. Performing first-principles calculations within the Density Functional Theory (DFT)[28,29] and employing the projector augmented plane wave method,[30] they calculated how the impurity modifies the local electronic density of states (LDOS), magnetic moments, and spin–orbit coupling. By analyzing how these modifications alter the exchange and DM energies in the EHH of a single skyrmion in a clean system, some conclusions are outlined. Namely, when Mn is substituted by Zn or Ir and Si by Pb, respectively, the interaction between defect and skyrmion is attractive, indicating the pinning of the magnetic texture. However, for Mn substituted by Co, the interaction between the defect and the skyrmion is weakly repulsive.

Lima Fernandes *et al.*[23] and Gede Arjana *et al.*[24] explained other examples where defects modify the material structure but, now, by the addition of new atoms. Both works used DFT, with the all-electron full-potential scalar-relativistic Korringa–Kohn–Rostoker (KKR) Green function method,[31,32] for the calculations of LDOS and magnetic moment modifications. In Ref. 23, the impact of single atomic defects on single magnetic skyrmions generated in PdFe bilayer deposited on Ir(111) surfaces is addressed. These atomic defects are 3d transition metals (Sc, Ti, V, Cr, Mn, Fe, Co, and Ni) and 4d transition metals (Y, Zr, Nb, Mo, Tc, Ru, and Rh) and Cu and Ag atoms either located on top of (adatoms) or embedded in (inatoms) the Pd surface layer [see Fig. 1(a)]. After mapping the magnetic exchange interactions from *ab initio* to a generalized Heisenberg model, some insights can be deduced. In general, in both inatoms and adatoms, with some exceptions, the 3d series tend to repel the skyrmion in contrast to those of the 4d series, Cu and Ag, which act as pinning centers [see Fig. 1(b)]. On the other hand, Ref. 24 investigates the energy profile of a single skyrmion at the vicinity of defects (dimer, trimers, and tetramers) of different shapes, sizes, and chemical nature (Cr or Fe) deposited on the PdFe/Ir(111) surface. The results of the EHH with the parameters extracted from DFT reveal that, besides the chemical nature of the impurities, the shape, size, and stacking of the defects are also essential elements to tune the energy landscape of magnetic skyrmions governed by the interplay of impurity–substrate and the impurity–impurity magnetic interactions.

In addition to the one discussed above, there is another way to simulate defects at the atomic scale. This second option consists of locally modifying the magnetic interaction constants (J, d, k) or directly modifying some of the magnetic moments of the lattice. To carry it out, it is not necessary to go to first-principles calculations to obtain the magnetic moments and magnetic interactions between neighboring atoms, being sufficient to use their experimentally obtained values. The works of Stosic *et al.*[25] and Navau *et al.*[26] are examples of defect simulations as changes on the interaction constants. Reference 25 investigates the pinning of magnetic skyrmions in a monolayer of the Co film on Pt(111) due to atomic defects of different nature. The magnetic material is simulated using EHH with values of material parameters obtained from experimental works listed in Ref. 20. The pinning of the skyrmion is analyzed by estimating the minimum energy paths of the pinned-unpinned states transitions by employing the Geodesic Nudged Elastic Band (GNEB) method.[33] Defects are considered as local variations in the form of step functions of J, d, and k in a set of chosen lattice points, and the rest of the sample is unchanged. The results show that, depending on the defect type and the ratio of skyrmion core to defect size, the skyrmion can be pinned at the skyrmion center, at the domain wall of the skyrmion core, or in between these two. For example, a defect simulated as a local reduction of anisotropy (50%) or exchange interaction (10%) produces the pinning of the skyrmion at its domain wall; however, a local increase of the DM interaction (100%) produces the pinning between the center of the skyrmion and the domain wall. In addition, this pinning position changes with the size of the skyrmion. That is, a defect induced by a variation in the exchange or DM interaction would pin the skyrmion at its center for small skyrmions, but off-center for large skyrmions. For anisotropy defects, the pinning is always off-center. When a linear defect (a set of aligned defects) is studied, all these behaviors on the pinning position are kept except in the case of linear defects induced by varied DM interaction, which can only pin a skyrmion at its center. It is found that defects also produce variations on the skyrmion shape; in particular, defects induce a breathing behavior on skyrmions: the skyrmion expands as it approaches a defect and then shrinks back to its original size at the pinning position. In addition to all the results already discussed, by analyzing how the skyrmion energy changes as a function of the relative distance between the skyrmion and defect, Ref. 25 also gives analytical expressions of the effective pinning potentials. These potentials will be taken into account when the skyrmion dynamics, in the presence of defects, are examined on a scale larger than the atomic scale (this concept will be explained in more detail in Sec. III). These pinning potentials are well represented by a generalized Gaussian function of the defect-skyrmion distance in the case of centered pinning and by the same function, but shifted, in the off-center pinning case.

The work of Navau *et al.*[26] is another example of defects simulated as a modification of the interaction constants. Reference 26 does not study a specific magnetic material but a thin film of generic material with magnetic moments arranged on a squared lattice and with interfacial DM interaction. In this case, defects are considered as local modifications of the exchange, DM, and/or anisotropy interactions. These changes can be made in the magnetic interactions associated with a single atom (point defect), as can be seen in Fig. 1(c), or in the interactions of a set of aligned atoms ranging from $-\infty$ to ∞ (linear defect). The authors found the extra energy terms that must be added to the Hamiltonian (in EHH) of the pristine sample (without defects) due to the presence of the point or linear defect of different kinds. From these extra energy terms, analytical expressions of the effective magnetic fields and effective forces, which are associated with the defect and act over the skyrmion, can be derived. The forces acting over the skyrmion are found to be proportional to the interaction constants' variation ratio. These forces will be useful to study defect effects on the skyrmion dynamics in the rigid approximation[34] (see Sec. III). Depending on the defect type, that is, point or linear defect with an increase/decrease of the different interactions (exchange, DM, or anisotropy), an attractive or repulsive force can be obtained. For example, in the case of point

defect, a local increase of the DM interaction induces an attractive force over the skyrmion. However, a point modification of the anisotropy constant produces an attractive force at low skyrmion-defect distances (compared with the skyrmion radius) but repulsive at large separations, and a point modification of the exchange interaction results in zero extra force. In the case of linear defects, local modifications can be made in the interactions between defect–defect and non-defect–defect atoms. When the modification is produced in the DM constant, only the changes in the interactions between atoms within the defect result in an effective force, being attractive when the interaction is increased. In the case of an exchange linear defect, an attractive force appears when the exchange interaction between defect atoms is larger than the interaction between non defect–defect atoms. The results obtained for an anisotropy linear defect are similar to the ones obtained in the point defect, that is, when the anisotropy constant is reduced, a repulsive force results for large skyrmion-defect separation, whereas an attractive one appears for small distances.

The example of Potkina *et al.*[27] is different from the above cases. In Ref. 27, the defect is simulated as a direct modification of the atomic magnetic moments. In particular, Ref. 27 studies the interaction of skyrmion with a non-magnetic impurity inside a track of different widths in a PdFe bilayer on Ir(111). The defect consists of 1, 3, 4, 7, and 8 vacancies without magnetic moment that form a compact group on a two-dimensional triangular lattice. The effects of the impurities over the skyrmion are analyzed by using EHH with the parameters values corresponding to experimental skyrmionic systems,[35] and the transitions between skyrmion and ferromagnetic states are described by minimum energy paths, which are obtained by using a GNEB variant method. On the one hand, Ref. 27 shows that the track width significantly affects the skyrmion stability and the activation energies of pinning and depinning and concludes that the width of the track should be significantly greater than two skyrmion diameters. On the other hand, the effect of the non-magnetic impurity on the activation energies of annihilation/nucleation and pinning/depinning processes is also analyzed. The authors found that increasing the defect size not only increases both nucleation and annihilation barriers, favoring both formation and destruction of the skyrmion in the defect, but also increases the skyrmion attachment and detachment barrier, making the pinning stronger.

The work of Stosic *et al.*[25] also simulated defects by modifying the magnetic moments. In particular, a defect is modeled by removing a set of lattice sites and the corresponding bonds (anyone involving a missing atom). In this case, the preferable position of the skyrmion pinning can be either at the center or at the domain wall (off-center) depending on the ratio of skyrmion to hole size. The study of the skyrmion energy as a function of the skyrmion-hole distance shows that the skyrmion must overcome a weak energy barrier to transition from an unpinned to a pinned state. This means that the effective pinning potential for skyrmions in the case of holes in the magnetic material needs, in addition to the generalized Gaussian term, a decaying exponential term in order to describe this energy barrier. Sufficiently large vacancies can reduce the stability of the skyrmion even leading to its collapse. However, this stability can be improved by increasing the DM interaction in the vicinity of the vacancy, for example, by introducing a heavy-metal capping layer (a MgO capping patch on the Co film on Pt).

III. DEFECTS AT MICROMAGNETIC SCALE

A. Skyrmions in micromagnetism

When one wants to study ferromagnetic samples with sizes ranging from tens of nanometers to microns, the use of EHH is computationally prohibitive. In these cases, the micromagnetic model is employed,[17,18,36] which describes the ferromagnetic material by means of macroscopic properties that are averages of the fundamental atomic interactions. This model uses a continuous version of the material Hamiltonian that, in turn, includes a continuous version of the different interactions (exchange, DM, anisotropy, Zeeman, and magnetostatics). The model assumes that atomic magnetic moments have a classical behavior and the change in the direction between neighboring moments is small. In addition, micromagnetism also assumes a continuous magnetization function $\mathbf{M}(\mathbf{r})$, whose direction is an average of the atomic magnetic moments involved at the position $\mathbf{r}$ (in a certain volume) and with constant modulus M_S (the saturation magnetization) all over the ferromagnetic sample. The variation of this magnetization function respect to time results in the dynamics of the magnetic structures that can be formed in the material. This dynamics can be evaluated through the Landau–Lifshitz–Gilbert (LLG) equation,[37] which reads

$$\frac{d\mathbf{M}}{dt} = -\gamma\, \mathbf{M} \times \mathbf{H}_{\text{eff}} + \frac{\alpha}{M_S}\mathbf{M} \times \frac{d\mathbf{M}}{dt} + \mathbf{T}, \tag{2}$$

where $\gamma = 2.21 \cdot 10^5$ m A^{-1} s^{-1} is the gyromagnetic constant. α is a positive dimensionless constant (Gilbert constant) accounting for the damping of the precession of the magnetization around the axis defined by the direction of the effective field $\mathbf{H}_{\text{eff}}$. This effective field can be defined as

$$\mathbf{H}_{\text{eff}} = \frac{2A}{\mu_0 M_S^2}\nabla^2\mathbf{M} + \frac{2K}{\mu_0 M_S^2}\hat{u}_K(\mathbf{M}\cdot\hat{u}_K) + \mathbf{H}_d + \mathbf{H}_a + \mathbf{H}_{DM}, \tag{3}$$

which contains the magnetic fields associated with the different interactions, ordered from left to right, as exchange, uniaxial magnetocrystalline anisotropy, magnetostatics, Zeeman, and DM. A and K are the exchange and anisotropy constants, respectively, related to the atomic J and k by means of factors depending on the particular material lattice structure.[17] $\hat{u}_K$ is the anisotropy easy axis. Similar to the EHH formalism, in thin film samples, the demagnetizing field $\mathbf{H}_d$ mainly acts as a shape anisotropy[38,39] and can be included, renormalizing the anisotropy constant.[19,40] $\mathbf{H}_a$ is the external applied magnetic field. The DM effective field $\mathbf{H}_{DM}$ and the associated boundary condition[41] can be described by

$$\mathbf{H}_{DM} = \frac{2D}{\mu_0 M_S^2}[(\nabla\cdot\mathbf{M})\hat{z} - \nabla(\mathbf{M}\cdot\hat{z})], \tag{4}$$

$$\left.\frac{d\mathbf{M}}{dn}\right|_{\text{border}} = \frac{D}{2A}(\hat{z}\times\hat{n})\times\mathbf{M}, \tag{5}$$

when there is an interfacial DM interaction, with $\hat{z}$ being normal to the interface, and

$$\mathbf{H}_{DM} = -\frac{2D}{\mu_0 M_S^2}\nabla\times\mathbf{M}, \tag{6}$$

$$\left.\frac{d\mathbf{M}}{dn}\right|_{\text{border}} = \frac{D}{2A}(\mathbf{M}\times\hat{n}), \tag{7}$$

when there is bulk DM interaction. In both cases, $\hat{n}$ is the direction of the edge normal and D is the DM constant that, as above, is related to the atomic d.[42] It has been experimentally observed that in multilayer systems, where thin ferromagnetic layers are sandwiched between asymmetric non-magnetic heavy metals, D increases at all the interfaces.[13] In most cases, these multilayer systems are treated with an effective global D (in some cases, other constants are also considered as effective ones[43]).

Once the effective field has been obtained, the energy density of the system $\mathscr{E}$ can be calculated as

$$\mathscr{E} = -\frac{1}{2}\mu_0 \mathbf{M}\cdot(\mathbf{H}_{\text{exch}} + \mathbf{H}_K + \mathbf{H}_d + \mathbf{H}_{DM} + 2\mathbf{H}_a), \tag{8}$$

where $\mathbf{H}_{\text{exch}}$ and $\mathbf{H}_K$ are the exchange and anisotropy magnetic fields, respectively, of Eq. (3). In theoretical simulations, typically, the magnetic moment structure of the system can be obtained by minimizing the micromagnetic energy analytically, for example, by assuming a one-dimensional system with cylindrical symmetry,[41] or numerically. In contrast, the dynamics of spin configurations are obtained by solving numerically Eq. (2). The most common method, which is the one used by the commercial software OOMMF[44,45] and MuMax,[46,47] is using a finite difference scheme and a high order time integrator, such as fourth-order Runge–Kutta (RK4) method. To ensure a good resolution of the micromagnetic framework, in the numerical cases, the sample discretization (meshing) must be done with cells of sizes smaller than the exchange length[17] defined by $l_{ex} = \sqrt{\frac{2A}{\mu_0 M_S^2}}$.

In the last term of Eq. (2), $\mathbf{T}$ represents extra torques[48,49] that could drive the skyrmion and affect the magnetization distribution. One example is the spin-transfer torque (STT). In this case, an in-plane current density $\mathbf{J}_F = J_F\hat{\phi}$ ($\hat{\phi}$ has only $\hat{x}$ and $\hat{y}$ components) flows through the ferromagnet, and its conduction-electron spins align in the direction of the local magnetization (adiabatic approximation), resulting in a reaction torque over the magnetization,[50]

$$\mathbf{T}_{STT,ad} = \frac{\mu_B P J_F}{e M_S}(\hat{\phi}\cdot\nabla)\mathbf{M}, \tag{9}$$

where μ_B is the Bohr magneton, e (>0) is the charge of the electron, and P is the spin-polarization factor of the current. In the case where there is some spatial mistracking in the alignment (non-adiabatic approximation), an extra torque term appears, given by[37,51]

$$\mathbf{T}_{STT,non-ad} = -\beta\frac{\mu_B P J_F}{e M_S^2}\mathbf{M}\times(\hat{\phi}\cdot\nabla)\mathbf{M}, \tag{10}$$

where β is a dimensionless constant accounting for the nonadiabaticity of the spin alignment with the local magnetization.

Another example of torque which can drive a skyrmion is the one generated by the spin-Hall effect (SHE). In this case, the skyrmion is driven after feeding an in-plane current density $\mathbf{J}_H = J_H\hat{\eta}$ ($\hat{\eta}$ has only $\hat{x}$ and $\hat{y}$ components) on the heavy metal, and the SHE generates an accumulation of electrons with spin polarized along $\hat{\sigma} = \hat{z}\times\hat{\eta}$ on the interface between the heavy metal and the ferromagnet. These spin-polarized electrons diffuse into the ferromagnet, generating a damping-like torque, given by[52,53]

$$\mathbf{T}_{SHE} = -\frac{\mu_B \theta_H J_H}{e M_S^2 Z}\mathbf{M}\times[\mathbf{M}\times\hat{\sigma}], \tag{11}$$

where Z is the ferromagnet thickness and θ_H is the Hall angle, which represents the ratio between the electronic current density through the heavy metal and the spin-polarized current density diffusing through the ferromagnet.

When a spin-polarized current density $\mathbf{J}_{OOP} = J_{OOP}\,\hat{z}$ is vertically (out of plane) injected into the ferromagnet, a similar torque to the one above occurs. This out-of-plane damping-like torque (OOPT) is given by[54]

$$\mathbf{T}_{OOP} = -\frac{\gamma\,\hbar\,J_{OOP}\,P}{2eM_S^3 Z}\mathbf{M}\times[\mathbf{M}\times\hat{p}], \tag{12}$$

where $\hbar$ is the reduced Planck constant and $\hat{p}$ is the unit polarization vector (only in-plane direction). Again, P is the spin-polarization factor of the current density.

In this micromagnetic framework, defects can be simulated basically in two different ways, either by locally modifying the geometry, such as by incorporating holes, protrusions, and depressions into the ferromagnetic material, or by modifying the value of the different interaction constants A, K, D. In both simulated approaches, the number of magnetic moments involved in the modifications will depend on the relation between defect and skyrmion sizes. In the following, we show examples of these two types of defect simulations.

1. Geometrically induced defects

Similar to the atomic defects of Sec. II, in order to simulate holes, one or more magnetic moments (micromagnetic spins in this case) are removed. The cases of Müller and Rosch,[55] Iwasaki *et al.*,[56] and Suess *et al.*[57] are different examples of how to consider holes. In the first case, the zero magnetic moments are located in the inner part of the ferromagnetic material, while in the other two cases, they are located at the edge. In the case of Ref. 55, the defect, with small radius as compared with the skyrmion radius, is incorporated as a missing spin, by setting $\mathbf{M} = 0$, in a generic ferromagnetic monolayer material of squared lattice with interfacial DM interaction. The effects of this single-site vacancy on the motion of a single skyrmion driven by STT are studied by solving the LLG equation. The results show that depending on the applied magnetic field and current density, the skyrmion could be captured by the hole or overcome it.

The simulated hole in Ref. 56 is a rectangular notch, larger than the skyrmion size, placed in one of the edges of a MnSi nanotrack modifying the contour of the sample. The hole is considered as a set of micromagnetic sites with $\mathbf{M} = 0$, and the dynamics of the system is obtained by solving the LLG equation taking into account STT and an applied magnetic field. The results of Ref. 56 show that the creation of skyrmions at the notch is possible depending on the spin-polarized current density and the applied magnetic field. The essential mechanism for the skyrmion nucleation is the in-plane components of the spins along the notch and their shift due to the spin-transfer torque.

The case of Ref. 57 is another example where notches of null magnetization are incorporated into one of the lateral boundaries. In Ref. 57, a racetrack of a Pt/Co/Ta multilayer is simulated and semicircular holes (larger than the skyrmion) are introduced in one edge in order to create pinning sites as a consequence of the geometrical constrictions. The results show that the energy barrier to overcome

these pinning sites is larger than the energy barrier for skyrmion annihilation in the investigated structure, that is, skyrmions have a tendency to lose their topological stability and to dissolve when they interact with these notches.

The effects of the geometrical constrictions caused by notches are also useful in some proposals for skyrmion logic systems.[58,59] In the system of Ref. 59, triangular notches are inserted at one edge of the different nanowires composing the logic device. These notches allow for skyrmion passage only when a large current density is applied. With this, the required synchronization between the skyrmions of different branches can be achieved. In the proposal of Ref. 58, rectangular notches are incorporated into the ferromagnetic sample to adjust the trajectories of the skyrmions and ensure the collision between them, enabling the logic operation altogether.

As an example of hole simulation, in Fig. 2, we can see the effects that a squared hole with size of the order of the skyrmion can produce over the skyrmion. In this case, the hole is simulated as a region with $\mathbf{M} = 0$ and the numerical results are obtained by solving the LLG equation with SHE (as in Ref. 60). Figure 2 shows how the z-component of the magnetization and the trajectory of a skyrmion are modified by the hole. In Fig. 2, we can see that this hole provides a repulsive effect over the skyrmion, pushing it in the vertical (positive y) direction. At the same time, the size of the skyrmion becomes smaller as it approaches the hole and returns to its original size as it moves away.

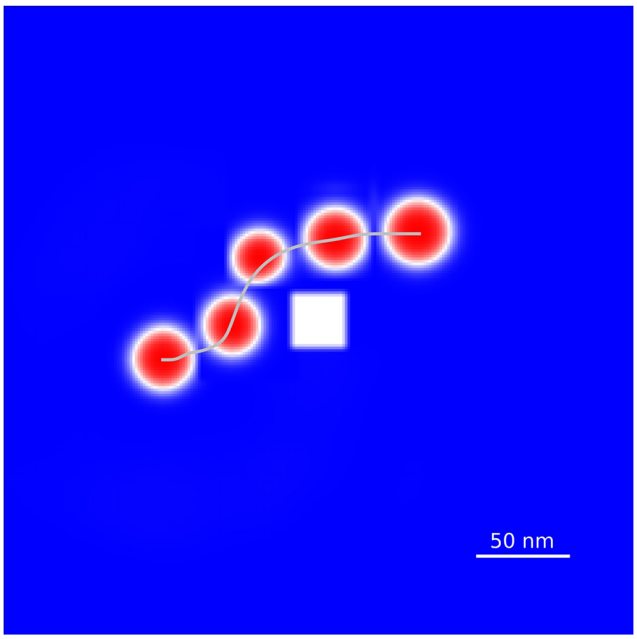

FIG. 2. Snapshots of the z-component of the magnetization (in units of M_s; blue, white, and red indicate +1, 0, and −1, respectively) at different times (from left to right, t = 0, 2.50, 3.75, 4.19, and 6.25 ns) when a squared hole of side 33.6 nm ($4l_{ex}$) is present. The xy-plane is plotted, with the horizontal (vertical) direction corresponding to the x (y) axis. The gray line describes the trajectory of the skyrmion. The numerical results are obtained by solving the LLG equation with a spin-polarized current (SHE) with $\theta_H J_H$ = 20 GA/m^2 flowing in the y direction and polarized in the x direction. The numerical method and parameters are the same as in Ref. 60.

In addition to holes, other geometry-induced defects can be considered, such as local thickness modulations, depressions, or protrusions (see Fig. 3). The case of Pathak and Hertel[61] is an example where the ferromagnet thickness is locally modulated. In Ref. 61, a FeGe film is modeled with the defects simulated as small cylindrical regions, with radius slightly larger than the radius of the skyrmion core, where the thickness of the host material is reduced by half through two cylindrical pockets inserted symmetrically on both top and bottom surfaces. By solving the LLG equation with micromagnetic finite-element simulations, the authors showed that these nano-pockets favor the stabilization of the skyrmions and act as capturing sites [see Fig. 3(a)]. This gives the possibility to control the position of skyrmions at predefined positions.

Recent works show that curvatures introduce changes in the properties of skyrmions. These modifications allow for the stabilization of skyrmions in conditions that are not propitious for planar geometry. That is, effective interactions of exchange, anisotropy, DM, and magnetostatics[64–67] can be induced by curvilinear geometries. For this reason, introducing defects with a certain curvature can also produce interesting effects. In the works of Kravchuck *et al.*[62] and Carvalho-Santos *et al.*,[63] we can find examples of curvilinear defects under static and dynamic conditions, respectively. In both cases, the continuous magnetization function, which characterizes micromagnetic theory, is reformulated in terms of the orthonormal curvilinear basis and the different micromagnetic energy terms are rederived.[68] In Ref. 62, the energy of the system is analytically studied when a single curvilinear defect (a Gaussian bump) or a periodically arranged square lattice of these bumps is incorporated into the ferromagnetic material. The authors found that, in a wide range of geometrical and material parameters and at the zero applied field, a skyrmion pinned on the bump has lower energy than the other possible states [see Fig. 3(b)]. Hence, curvilinear defects arranged in a periodical lattice generate a zero-field Skyrmion lattice as a ground state of the system.

In Ref. 63, the authors studied the skyrmion propagation along a FeGe nanostrip with a curved section consisting of a hill in the film's central region [see Fig. 3(c)]. The dynamics of the skyrmion is obtained by solving the LLG equation with STT by using MuMax3, and the curved nanostrip is described by a combination of hyperbolic tangent functions, which depends on the geometry of the hill (height and extension). The results show that the protuberance creates a curvature-induced effective force capable of stopping the skyrmion. Depending on the value of the DM constant and the driving current density, the skyrmion can stop at the flat region (before the hill) or at the curved region, or it can overcome the hill and cross the full rail.

2. Defects as modifications of the interaction constants (A, K, D)

Another way to model defects in the micromagnetic scope is to locally alter the constants associated with the different interactions between the magnetic moments, describing the ferromagnetic system. Two options of carrying out these modifications can be found in the literature. The first option consists of introducing that, at a specific location in the lattice (defect center), the constant follows

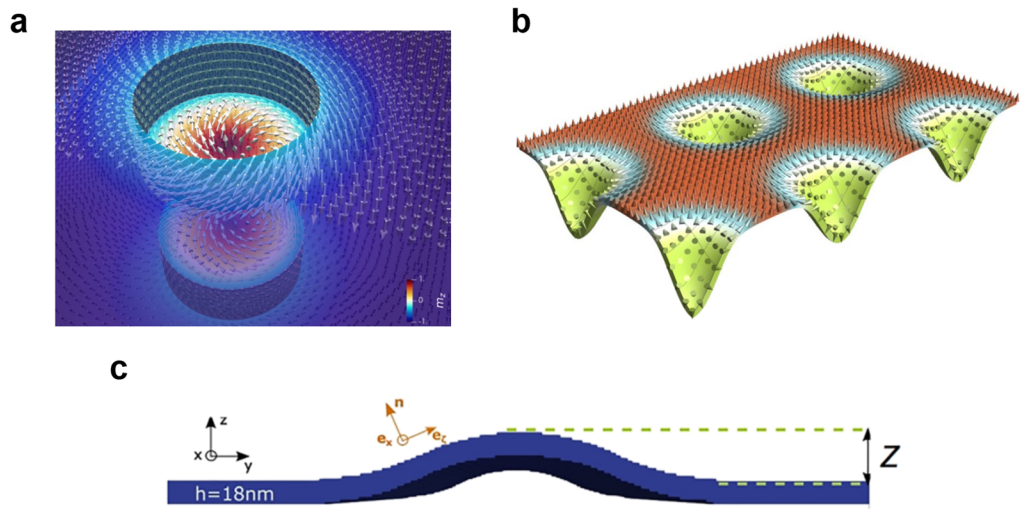

FIG. 3. Some examples of geometrically induced defects. (a) A cylindrical region where the thickness is reduced by half through two cylindrical pockets inserted on both top and bottom surfaces [reproduced with permission from S. A. Pathak and R. Hertel, Magnetochemistry **7**, 26 (2021). Copyright 2021 Author(s), licensed under a Creative Commons Attribution (CC BY) license]. (b) A periodically array of curvilinear bumps incorporated into the ferromagnet in which the skyrmion lattice is the ground state [reproduced with permission from Kravchuk *et al.*, Phys. Rev. Lett. **120**, 067201 (2018). Copyright 2018, American Physical Society]. (c) A hill in the ferromagnetic nanostrip [reproduced from Carvalho-Santos *et al.*, Appl. Phys. Lett. **118**, 172407 (2021) with the permission of AIP Publishing].

a mathematical function that varies with distance, such as Gaussian functions[69,70] or exponential decays,[71] in regions smaller than or similar to the skyrmion size. Specifically, in the case of Hanneken *et al.*,[69] the skyrmion pinning in PdFe on Ir(111) is studied. With constant-current Scanning Tunneling Microscopy (STM) images, they were able to see four single atom inlayer defects (presumably single Fe atoms) in the Pd layer, while in the Fe layer, the skyrmions are present. Depending on the position where the skyrmions are pinned and using micromagnetic energy calculations, Ref. 69 predicts what kinds of defects (exchange, DM, or anisotropy) exist in the real sample. Each type of defect is modeled by considering the interaction constant (A, D, or K) as a Gaussian function with 10% reduced value. Then, the energy of the system is calculated as a function of the skyrmion-defect distance. The results show that an off-center defect configuration can be due to either decreased A or increased D for large skyrmions (when the applied magnetic field is 1 T) or a smaller K of the defect with respect to the environment for both small (when the applied magnetic field is 3 T) and large skyrmions.

In the work of Liu and Li,[70] we found another example where defects are simulated as Gaussian-like variations of the interaction constants. In particular, Ref. 70 proposes a mechanism to pin skyrmions in chiral magnetic thin films by introducing Gaussian functions in both the exchange and DM constants as pinning centers. The ratio A/D remains constant, and the Gaussian-function amplitude allows us to locally increase the value of the constants up to 50% or 100%. This kind of defect is justified by the inhomogeneities in the local density of itinerant electrons.[72] In the stationary regime, they studied the pinning process calculating the changes on skyrmion energy as a function of the defect strength (Gaussian amplitude) and the applied magnetic field when the defect size (Gaussian variance) is similar to the skyrmion size. When the strength increases, the pinning also increases, that is, the energy of the skyrmion decreases, and a larger applied magnetic field is needed for skyrmion to evolve to the ferromagnetic state. The skyrmion motion caused by a single defect is analyzed with the LLG equation, and the defect is introduced in the effective field as a Gaussian function for A and D. This results in a skyrmion trajectory, which is a circular motion around the pinning center with the distance to the pinning center becoming smaller and smaller (spiral motion) that finally ends at the pinning center.

The work of Lin *et al.*[71] is slightly different from the two works just discussed. The skyrmion pinning in metallic chiral magnets (with magnetic values compatible with MnSi) is studied, and the defects are modeled as a local maxima of the exchange constant, that is, $A(\mathbf{r}) = A_{\text{norm}} + \sum_i A_d \exp(-|\mathbf{r} - \mathbf{r}_{d,i}|/\xi_d)$. A_{norm} is the exchange constant of the sample without defects, A_d characterizes the strength of the defects (variation of 10% or 30% from A_{norm}), $\mathbf{r}_{d,i}$ is the ith pinning-center position, and ξ_d is the characteristic size of the defects, which is comparable to the interatomic separation. By analyzing the change in the skyrmion energy as a function of the distance between skyrmion and defect, the authors found the attractive/repulsive nature of the defects as a function of the different parameters (A_d and ξ_d).

The second option to introduce a defect by modifying the interaction constants is based on considering that in a certain region, typically larger than the skyrmion size, these constants have fixed values but are different (large or low) from the rest of the ferromagnetic material.

In this way, Toscano *et al.*[73] compared how skyrmions are influenced by defects of different nature. These defects, which are located in the neighborhood of the skyrmion, are modeled as squared

regions with variations (±30%) on the magnetic material parameters, such as A, D, K, and M_S. The LLG equation without the influence of an external agent, such as magnetic fields or spin-polarized currents, is numerically solved. Typical parameters for Co/Pt multilayers are chosen. The results conclude that, whenever the defect size was larger than the skyrmion size, any of the modified magnetic parameters can be used to create both pinning and scattering traps by tuning either a local increase or a local decrease of a given magnetic property. With no external agent other than the defect, the skyrmion moves either toward the defect, when attracted by a pinning trap, or away from the defect, when repelled by a scattering trap.

The works of Sampaio *et al.*[16] and Ding *et al.*[74] are examples where large defects of anisotropy are considered. In both cases, skyrmions move along a magnetic nanotrack (Pt/Co system[75]) because of the effect of a vertically injected spin-polarized current (OOPT) from the heavy metal to the ferromagnetic layer. Defects are repulsive triangular notches of stronger perpendicular anisotropy (50% and 33% stronger compared with the rest of the sample for Refs. 16 and 74, respectively). This kind of defect could be obtained, for example, by ion radiation.[76] The skyrmion dynamics are obtained by solving the LLG equation, including spin–orbit torque, using OOMMF. On the one hand, in Ref. 16, the behavior of a single skyrmion is analyzed for different notch depths, showing that depending on the current density, the skyrmion stops when it runs into the notch or, for larger current densities, moves around the notch and continues on its initial trajectory with its initial velocity. On the other hand, in Ref. 74, a chain of two skyrmions is considered to study the effect of the repulsive interaction between skyrmions with the above geometry. In addition to the results in which both skyrmions pass or are blocked, a third case is obtained. That is, the first skyrmion is blocked when it reaches the notch, but when the second skyrmion approaches the first one, which remains pinned, the repulsion between them causes the first skyrmion to pass and move away from the defect, while the second skyrmion is now the one trapped. Repeating the calculations for different H_a and different K, it is observed that the smaller the skyrmion, the lower the current density required to free the two magnetic structures.

The work of Everschor-Sitte *et al.*[77] is another example where an anisotropy defect is analyzed, but, in this case, not only the value of the constant is reduced but also the uniaxial direction of anisotropy is changed. In Ref. 77, a metallic ferromagnetic thin film with a perpendicular uniaxial anisotropy (parameter values compatibles with CoCrPt/Ti) is simulated with the defect modeled as a cylindrical small region with in-plane uniaxial anisotropy (with a value 80 times lower than the rest of the film). This defect with tilted anisotropy can be obtained, for example, by tuning one of the material layers.[78] With analytical and numerical calculations[46,47,79] of the LLG equation with STT, Everschor-Sitte *et al.* presents a mechanism for periodical nucleation of skyrmions based on the application of an in-plane homogeneous DC current. When the applied current J is above a critical current J_c, which is the needed current to push away the skyrmion due to STT, skyrmions are periodically created with a period proportional to $(J - J_c)^{-1/2}$.

Mulkers *et al.*[80] and Castell-Queralt *et al.*[60] are examples of defect simulations as modifications on the DM interaction constant. In both works, defects are specially designed to promote or improve some of the skyrmion properties, such as its velocity and trajectory. On the one hand, in Ref. 80, the aim is to improve the skyrmion confinement. The engineered defects are local modifications of the D strength. It is known that the effective DM interaction strength depends on the thickness of the ferromagnetic layer and the stacking of the ferromagnetic layer and heavy-metal layers.[81–83] This kind of defect could be included by using lithographic techniques to (partially) change or remove the heavy metal layer on top of the ferromagnet layer. By numerically minimizing the micromagnetic energy, Ref. 80 concludes that skyrmions can be very effectively confined inside the prepatterned regions with higher DM interaction, in particular, in a circular region with large D (up to 60% increase) surrounded by an extended region without DM interaction. The stronger the confinement (small radius of region with high D), the smaller the skyrmion radius. In addition to the above, an alternative racetrack to race skyrmions is proposed. The track is created by a high-DM strip in an extended ferromagnetic film, with weak or no DM interaction outside the strip. The LLG equation is numerically solved with MuMax3 for a single skyrmion moved by a spin-polarized current, taking into account parameter values of Co/Pt multilayers. The obtained results reveal that for current densities in which the skyrmion escapes from the conventional finite tracks, due to the interaction with the borders,[48,84–86] the skyrmion remains on the track in the case of high-DM interaction strip, reducing its volatility to collapse.

On the other hand, in Ref. 60, a platform to accelerate, guide, and compress skyrmions by defect rails is proposed. The rails consist of a pair of line defects, one of them is attractive (local increase, about 50% or 70%, of interfacial DM interaction) and the other is repulsive (local reduction, about 50% or 70%, of interfacial DM interaction). The system is modeled as a planar ultrathin ferromagnetic film on top of a non-magnetic heavy metal, and its dynamics is obtained by numerically solving the LLG equation taking into account SHE using typical parameters of Co/Pt/AlO_x.[6,16,43] The obtained results show that, within a range of driving current densities and defect strengths, the skyrmion is guided along channels with a width of the order of the radius of the initial skyrmion. At the same time, the skyrmion speed is enhanced by an order of magnitude. The work of Castell-Queralt *et al.* provided a new strategy for enhancing the transport stage because being guided, accelerated, and compressed, the amount of skyrmionic information that can be transported for a given total width of the film could be boosted.

Finally, to illustrate defects simulated as modifications of the interaction constants, we present Fig. 4. In Fig. 4, we show four different defects. Although in all cases the defect is a rectangular region (green line), in Figs. 4(a) and 4(c), the defect corresponds to a reduction of the DM and anisotropy constants, respectively. Instead, in the rectangular defect of Figs. 4(b) and 4(d), D and K are increased, respectively. Note that in Figs. 4(a) and 4(c), and Figs. 4(b) and 4(d), K and D modifications have opposite behaviors over the skyrmion evolution and trajectory. When the DM constant is reduced (15%), Fig. 4(a), the skyrmion trajectory is deflected upward and its size is slightly reduced near the defect (similar to the hole case of Fig. 2) because of the repulsive effect of the rectangular region. However, in the case of anisotropy-modification defect, this behavior is observed when K is increased (10%), Fig. 4(d). In the same way, the attractive behavior observed in Fig. 4(b) when D is increased (5%), which is a downward

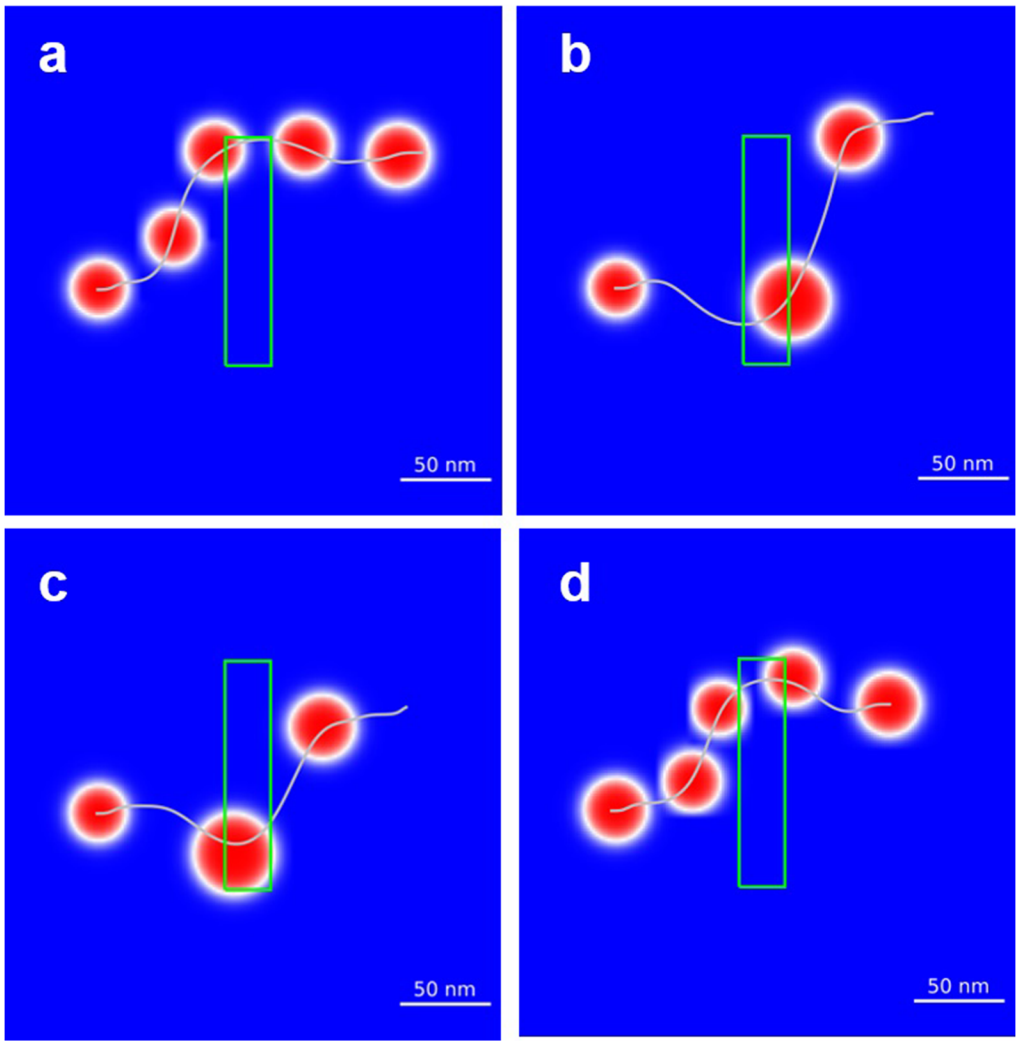

FIG. 4. Snapshots of the z-component of the magnetization (in units of M_s; blue, white, and red indicate +1, 0, and −1, respectively) at different times when a rectangular defect (delimited by the green line) of dimensions 25.2 × 126 nm^2 is present. (a) The rectangular defect is modeled as a reduction of the interfacial DM constant to the value $D_d = 0.85D_0$, where D_0 is the value of the constant in the rest of sample. The time steps are, from left to right, t = 0, 3.75, 5.62, 7.50, and 11.25 ns. (b) The rectangular defect is modeled as an increase of the interfacial DM constant to the value $D_d = 1.05D_0$, and the times are, from left to right, t = 0, 5, and 8.75 ns. (c) The rectangular defect is modeled as a reduction of the anisotropy constant to $K_d = 0.9K_0$, where K_0 is the anisotropy constant in the rest of sample. The time steps are the same as in (b). (d) The rectangular defect is modeled as an increase of the anisotropy constant to $K_d = 1.1K_0$, and the time steps are the same as in (a). In all cases, the xy-plane is plotted and the horizontal (vertical) direction corresponds to the x (y) axis. The gray line describes the trajectory of the skyrmion. The numerical results are obtained by solving the LLG equation with a spin-polarized current (SHE) with $\theta_H J_H$ = 15 GA/m^2 flowing in the y direction and polarized in the x direction. The numerical method and parameters are the same as in Ref. 60.

deflection in the skyrmion path and a growth of its radius near the defect, is similar to the one observed in Fig. 4(c) when the anisotropy constant is increased (10%).

B. Rigid model

The LLG equation describes the time evolution of the magnetization distribution of the system. However, in situations where the shape and size of a magnetic structure (in our case the skyrmion) do not change significantly, it is enough to describe the magnetization evolution as a global collective motion. This approach is known as the rigid model, described by Thiele's equation[34] which, apart from simplifying the calculations, allows us to obtain analytical expressions of the system dynamics in some cases. It is customary to use this model in ferromagnetic systems with thin planar geometries. The skyrmion is considered as a point quasi-particle with unaltered shape, neglecting internal degrees of freedom, and its dynamics is characterized by the movement of its center-of-mass position $\mathbf{r}_s$ (and velocity $\mathbf{v}_s$) on the xy-plane (the sample plane). That is, under the assumption of $\mathbf{M}(\mathbf{r}) = \mathbf{M}_0[\mathbf{r} - \mathbf{r}_s(t)]$, where $\mathbf{M}_0$

represents the magnetization distribution centered at $\mathbf{r} = 0$, and following the derivations in Ref. 34, Eq. (2) becomes

$$(\mathbb{G} - M_s\alpha\mathbb{D})\mathbf{v}_s + \gamma M_s^2\mathbf{F}_{\text{ext}} + \mathbb{B}\mathbf{v}_{\text{drv}} = 0. \quad (13)$$

The first term contains the Magnus and the dissipation (damping) terms that depend on the skyrmion velocity. $\mathbb{G}$ and $\mathbb{D}$ are constant matrices, which only depend on the internal characteristics of the skyrmion. They are defined as $\mathbb{G}_{uw} = \int_V \mathbf{M}_0 \cdot \left(\frac{\partial \mathbf{M}_0}{\partial u} \times \frac{\partial \mathbf{M}_0}{\partial w}\right) \mathrm{d}V$ and $\mathbb{D}_{uw} = \int_V \left(\frac{\partial \mathbf{M}_0}{\partial u} \cdot \frac{\partial \mathbf{M}_0}{\partial w}\right) \mathrm{d}V$, with u and w being x or y and V being the volume where the magnetization changes. The second term is due to external forces acting over the skyrmion, such as defects, borders, and potentials. These forces are defined as $(\mathbf{F}_{\text{ext}})_u = \int_V \mathbf{H}_{\text{ext}} \cdot \frac{\partial \mathbf{M}_0}{\partial u} \mathrm{d}V$, with $\mathbf{H}_{\text{ext}}$ being the effective external field due to external interactions. It is also common to express this external force as a potential gradient $(\mathbf{F}_{\text{ext}})_u = -(\nabla U)_u$. Finally, the last term of Eq. (13) arises from the torques of Eq. (2). $\mathbb{B}$ is another constant matrix, which depends on the skyrmion internal structure, but the exact expression depends on the torque type.[16,48–54] $\mathbf{v}_{\text{drv}}$ is the driving velocity, in the xy-plane, that different torques give to the skyrmion. For example, in the SHE case, where the skyrmion is driven after feeding an in-plane current density $\mathbf{J}_H$ in the heavy-metal substrate, $\mathbb{B} = M_S\mathbb{N}$ with $\mathbb{N}_{uw} = \frac{1}{Z}\int_V \left(\frac{\partial \mathbf{M}_0}{\partial u} \times \mathbf{M}_0\right)_w \mathrm{d}V$ and $\mathbf{v}_{\text{drv}} = -\frac{\mu_B \theta_H}{eM_S}(\hat{z} \times \mathbf{J}_H)$, where Z is the thickness of the ferromagnet. When the skyrmion is driven as a result of an out-of-plane current density $\mathbf{J}_{OOP}$, polarized along $\hat{p}$, $\mathbb{B}$ is again $M_S\mathbb{N}$, but the driving velocity is $\mathbf{v}_{\text{drv}} = -\frac{\gamma \hbar J_{OOP} P}{2eM_S^2}\hat{p}$. Another example is the STT case, where the skyrmion moves due to an in-plane current density $\mathbf{J}_F$ (adiabatic and non-adiabatic approximation), $\mathbb{B} = \mathbb{G} - M_S\beta\mathbb{D}$ and $\mathbf{v}_{\text{drv}} = -\frac{\mu_B P}{eM_s}\mathbf{J}_F$.

As mentioned above, in this rigid approach, the defects are incorporated into the system through the external forces term of Eq. (13). However, these effective forces (or potential gradients) can have different expressions depending on the nature and size of the defect, as will be discussed below.

1. Point defect as fitted effective potential/force

A way to incorporate the defects into Thiele's equation is by means of analytical expressions of external forces and potentials obtained by fitting some numerical values related, for example, to the energy of the skyrmion at different relative distances between the defect and the skyrmion. This is the case of Refs. 55 and 71 where, in addition to the study of the skyrmion's motion with the LLG equation (shown in Secs. III A 1 and III A 2), its dynamics is also studied with Thiele's equation. In the case of Ref. 55, the simulated defect is a hole and its effect is taken into account by means of an external potential with a long-range repulsion and a short-range attraction, which follows an exponential law for very large skyrmion-defect distance and polynomial otherwise. These dependencies are obtained by fitting the evolution of the skyrmion energy minima, which have been found previously by minimizing the energy with respect to the skyrmion-hole distance. The authors found that the effects of the vacancy can be classified into three types: the pinning case where a skyrmion freely moves around defects and never gets captured but stays pinned if it was initially pinned, the capturing case in which a moving skyrmion can get captured within a certain capturing cross section (proportional to the skyrmion size and to $\sqrt{\alpha}$), and the free case where a skyrmion can never be pinned by the vacancy.

In Ref. 71, an exchange defect is also incorporated into the Thiele equation by adding a fitted external force. One of the main results of Ref. 71 is to present an analytical expression for the interaction force between the skyrmion and a defect, which can be incorporated into the Thiele model. The force reads $\mathbf{F}_d = F_0 \exp(-r_{ds}/\xi_d)\hat{r}_{ds}$, where F_0 is the strength of the force (proportional to A_d), r_{ds} is the relative distance between the defect and the skyrmion, and $\hat{r}_{ds}$ is the unit vector along r_{ds}. This expression is obtained by evaluating how the skyrmion energy, which is computed with micromagnetic calculations, changes as a function of the skyrmion-defect distance.

2. Point defects as Gaussian potentials

When a defect is considered, for example, as a local variation of the DM interaction,[26] the force can be well approximated by a radially symmetric force, which linearly increases close to the pinning center and decays when far from it. An adequate potential for describing this force is a Gaussian function. In the case of a defect localized at the origin of coordinates, this Gaussian-like potential reads $U(\rho) = -U_0 \exp\left(-\frac{\rho^2}{\lambda_0^2}\right)$, where λ_0 (>0) is a parameter that indicates the radial scope of the defect (typically coinciding with the skyrmion radius), U_0 is its intensity, and ρ is the radial distance from the origin. In the case of an attractive defect $(U_0 > 0)$, the force created by this potential is $\mathbf{F}_{\text{ext}} = -f_0 \frac{\rho}{\lambda_0} \exp\left(-\frac{\rho^2}{\lambda_0^2}\right)\hat{\rho}$ with $f_0 = \frac{2U_0}{\lambda_0}$. The works of Refs. 49 and 70 are examples of Gaussian point defects. Both cases study the skyrmion dynamics by solving Thiele's equation, with STT for Ref. 70 and SHE for Ref. 49, obtaining equivalent results. The combination of electric-current pushing and defect forces results in a skyrmion trajectory, which is a spiraling motion around an attractor point (close to but not in the same position as the defect) where the skyrmion is finally trapped. In Fig. 5(a), we can see an example of this spiraling behavior in the skyrmion movement due to a Gaussian attractive point defect. In the case of low driving velocity (red line), the skyrmion is trapped close to the defect, but when the velocity is high enough (blue line), the defect attraction is unable to pin the skyrmion. Figures 5(b) and 5(c) show the vector fields corresponding to the defect force and the defect-induced velocity, respectively. The force arrows point to the defect (attraction), and the velocity vectors rotate counterclockwise. This explains the downward trajectory of the skyrmion and the rotation around the defect. By contrast, Fig. 6 shows the upward pushing effect of a repulsive point defect. As an example, in Fig. 7, we can see the effects on the skyrmion dynamics that a particular combination of both attractive and repulsive Gaussian point defects could induce.

The work of Castell-Queralt *et al.*[87] also simulates a single attractive defect as a Gaussian potential but at non-zero temperature. They studied how defects influence the skyrmion dynamics when thermal effects are included, which will be relevant to understanding the behavior of room-temperature skyrmions.[43] In Ref. 87, a deterministic, while probabilistic, approach is considered for studying the motion of skyrmions, including temperature. The studied system is a magnetic ultrathin film on top of a heavy-metal substrate with the skyrmion being driven through damping-like

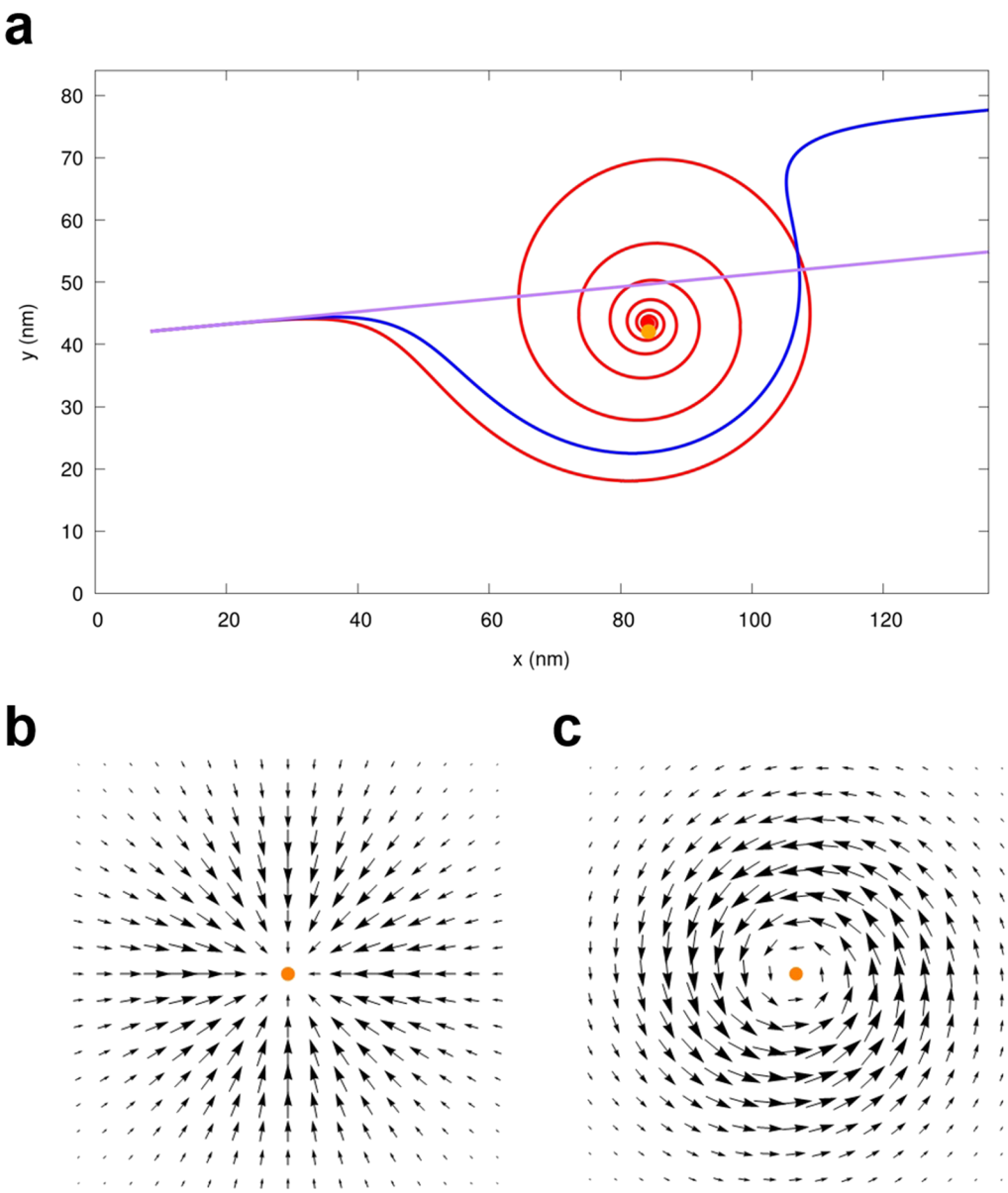

FIG. 5. (a) Thiele's trajectories of a skyrmion driven by SHE in the presence of an attractive Gaussian point defect (orange dot) with $f_0 = 4$ (normalized to $M_S^2 Z\lambda_0$) and $\lambda_0 = 21$ nm for the driving velocities ($\mathbb{N}\lambda_0 \mathbf{v}_H / M_S^2$) of 260 m/s (in red) and 520 m/s (in blue). The trajectory of the defect-free case is also plotted (in purple) for comparison. It is considered that $\mathbb{G}/M_S^3 Z = \mathbb{D}/M_S^2 Z = 4\pi$ and $\alpha = 0.3$. (b) Vector field corresponding to the force provided by the attractive Gaussian point defect. (c) Vector field corresponding to the velocity that the attractive Gaussian point defect gives to the skyrmion.

torques produced by spin-polarized currents and the SHE. The starting point is the stochastic Thiele equation[88,89] that is the same as Eq. (13) but adding the extra stochastic term $\gamma M_S^2 \mathbf{F}_{\text{st}}$ on the left part. $\mathbf{F}_{\text{st}}$ is considered a white noise with $\langle F_{\text{st},j} \rangle = 0$ and $\langle F_{\text{st},i} F_{\text{st},j} \rangle = \frac{2\alpha \mathbb{D} k_B T}{\gamma \mu_0 M_S} \delta_{ij} \delta(t - t_0)$, where $i, j = x, y, z$, T is the temperature, μ_0 is the vacuum permeability, k_B is the Boltzmann constant, δ_{ij} is the Kronecker delta, and $\delta(t - t_0)$ is the temporal Dirac's delta. As a Langevin equation, this stochastic equation has an associated deterministic Fokker–Planck equation[90] (see the supplementary material of Ref. 87 for details), which provides the probability density of finding the center of mass of the skyrmion at a given position and time. The advantage of using the Fokker–Planck equation is that by solving once, this single partial differential equation provides the same relevant probabilistic information as solving the stochastic Thiele

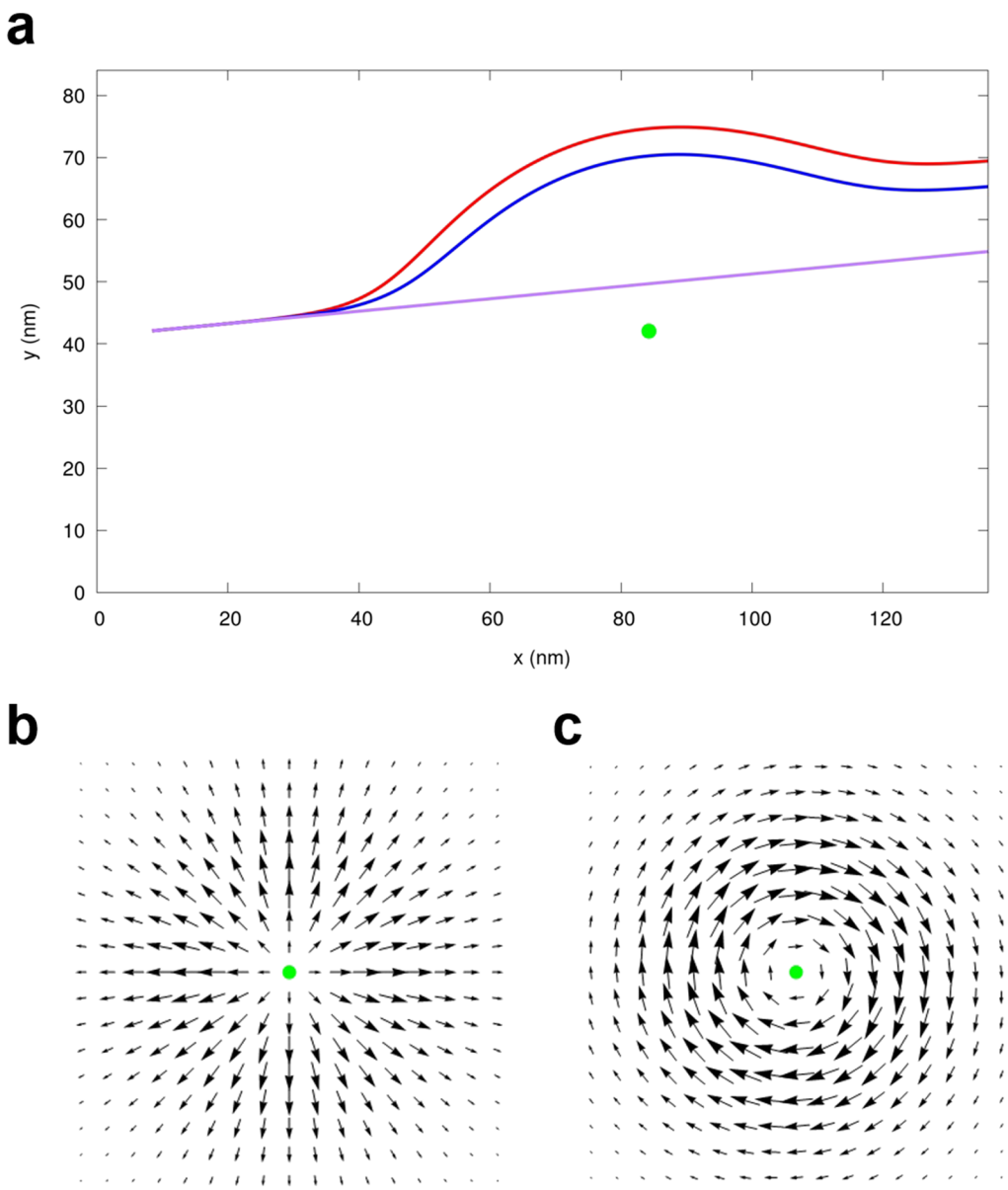

FIG. 6. The same as Fig. 5 but with a repulsive Gaussian point defect (green dot) with $f_0 = -4$.

equation many times. The results of Ref. 87 reveal that temperature is a factor that must be taken into account. Due to thermal diffusion, it is possible that a skyrmion that would escape at zero temperature does not when T increases or, the opposite, that a skyrmion that would be trapped at very low temperature has some "thermal chance" of escaping.

3. Potentials of extended defects

All the potentials discussed until now have simulated point or very localized defects (smaller than the skyrmion). However, under certain approximations, extended defects can also be considered as analytical potentials. González-Gómez *et al.*[49] and Martínez and Jalil[91] are examples of works with these kinds of potentials. On the one hand, González-Gómez *et al.* developed an analytical model of the skyrmion-defect interaction and, from this interaction and using Thiele's equation with SHE, described the trajectories and velocities of the skyrmions in the presence of large defects. From the Gaussian potential associated with a point defect (shown in Sec. III B 2), Ref. 49 provides analytical expressions of the interaction of extended defects, such as finite and infinite lines and combinations of these two, as can be cross-shaped, L-shaped, and grid

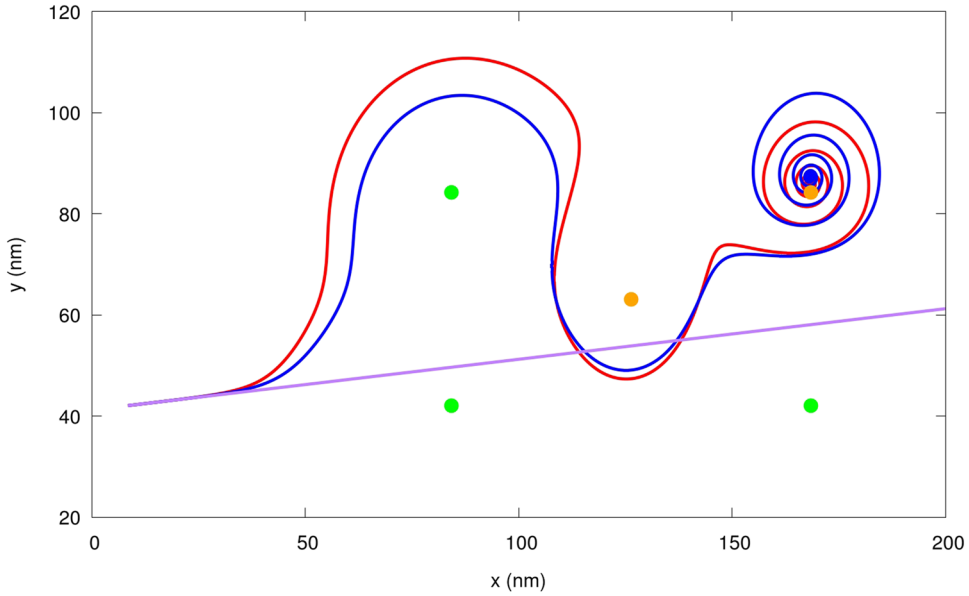

FIG. 7. Thiele's trajectories of a skyrmion driven by SHE in the presence of some repulsive (green dots) and attractive (orange dots) Gaussian point defects with $|f_0| = 4$ (normalized to $M_S^2 Z\lambda_0$) and $\lambda_0 = 21$ nm for the driving velocities ($\mathbb{N}\lambda_0 \mathbf{v}_H / M_S^2$) of 260 m/s (in red) and 520 m/s (in blue). The purple line corresponds to the defect-free case. It is considered that $\mathbb{G}/M_S^3 Z = \mathbb{D}/M_S^2 Z = 4\pi$ and $\alpha = 0.3$.

defects. These analytical expressions are obtained by integrating the contribution of many Gaussian point defects, which are very close one to each other, that is, the distance between two consecutive point defects (Δ) is much lower than the total length of the extended defect. To confirm the validity of the analytical results, some micromagnetic calculations from the LLG dynamical equation were performed with the home-made code of Ref. 60, showing a good agreement. In particular, Ref. 49 finds that skyrmions can either cross line defects and be trapped by or guided along them depending on the initial relative skyrmion-defect position, defect length, and the applied current density (direction and strength). In the case of a grid-like defect, skyrmions can be arranged in periodic positions. The advantage of being analytical results is that the points where skyrmions are trapped, the guiding velocity along defects, or the conditions for such trapping to exist, can be obtained as a function of the relevant parameters of the system. These parameters not only include the forces generated by the defects but also the controllable agents capable of driving the skyrmions. Figure 8 shows examples of skyrmion trajectories for different driven velocities in the case of an extended attractive defect (finite-line defect).

On the other hand, Ref. 91 studies the Thiele equation for current-induced motion (STT) in a skyrmion through one-dimensional sinusoidal and two-dimensional exponential-law potentials. The Thiele equation is composed of a Magnus force (topological origin), responsible for transverse motion relative to the current velocity, a dissipation force along the current velocity, and the pinning force (defect origin). In the one-dimensional potential, the results show that Magnus force dominates the dynamics even in the transverse motion. The velocity below which motion in the current direction is not allowed is interpreted in terms of the balance between the Magnus and the pinning forces. In the two-dimensional potential case, the occurrence of straight trajectories evidences the interplay of the Magnus and dissipative forces. To obtain a pinning onto a point, two attractive potentials separated from each other have to be considered.

IV. DISORDERED AND GRANULAR MATERIALS

It is well known that when a spin-polarized current density is applied to drive skyrmions, there exists a critical or threshold current density at which the motion starts. This critical-current density, which is orders of magnitude lower in the case of skyrmions than in the case of domain walls,[3,4] is a consequence of the presence of intrinsic impurities or defects in the skyrmion-carrying material. In the literature, one can mainly find two different ways to simulate disordered materials. The first one is to simulate this disorder by incorporating a set of defects, which can be, for example, local anisotropy defects[5,92] or effective skyrmion-defect forces[55,93–100] in the micromagnetic regime and in the Thiele approximation, respectively. These defects can be randomly or periodically distributed and have identical or slightly different properties. The second way to simulate the intrinsic pinning of materials is to consider the ferromagnetic sample as granular. That is, the ferromagnet is composed of grains with different sizes, and each grain can be considered as a different defect.[101–107] In the following, we show some examples of both disorder simulation approaches.

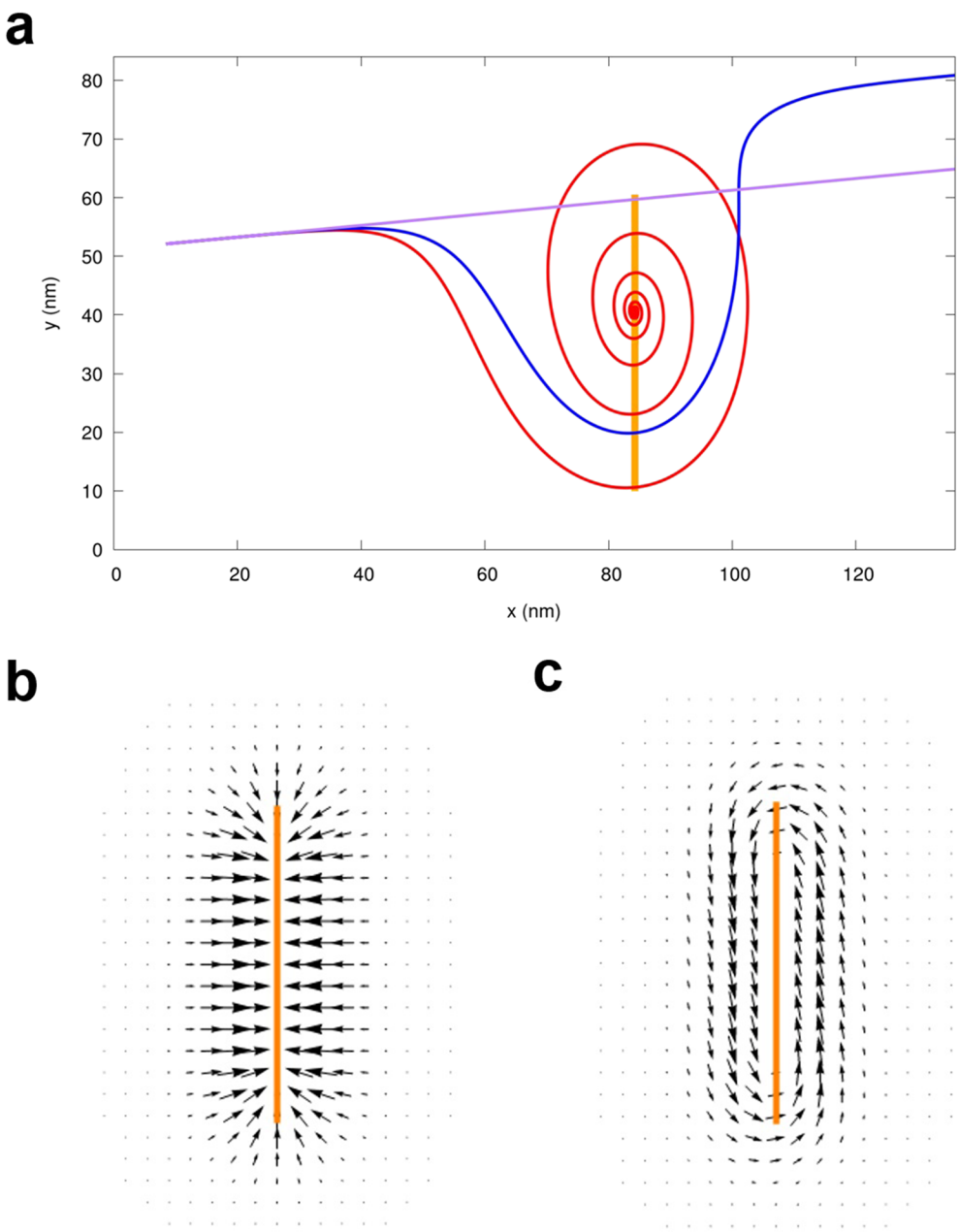

FIG. 8. (a) Thiele's trajectories of a skyrmion driven by SHE in the presence of an attractive finite-line defect (orange line) for the driving velocities ($\mathbb{N}\lambda_0 \mathbf{v}_H/M_S^2$) of 260 m/s (in red) and 520 m/s (in blue). The trajectory of the defect-free case is also plotted (in purple) for comparison. The defect length is 50.4 nm ($6l_{ex}$), and the finite-line defect is simulated following Eq. (21) of Ref. 49 with $f_0 = 4$ (normalized to $M_S^2 Z\lambda_0$), $\lambda_0 = 21$ nm, $\Delta = 0.054$ nm, $\mathbb{G}/M_S^3 Z = \mathbb{D}/M_S^2 Z = 4\pi$, and $\alpha = 0.3$ among other parameters. (b) Vector field corresponding to the force provided by the attractive finite-line defect. (c) Vector field corresponding to the velocity that the attractive finite-line defect gives to the skyrmion.

A. Disorder incorporated with a set of defects

When the disorder is due to many defects, we can classify the different theoretical works into two groups depending on the framework used: those that consider anisotropy defects (micromagnetism) and those that consider effective potentials (Thiele's approximation).

1. Set of anisotropy defects

Within this group, we find the works of Iwasaki *et al.*[5] and Koshibae and Nagaosa.[92] In the case of Ref. 5, the authors gave a theoretical explanation on why the spin-polarized current densities needed to drive skyrmions are much smaller than the ones needed for domain walls. Additionally, the effect of the material

intrinsic impurities on the critical-current density is explained. To carry out this theoretical study, two ultrathin plane chiral-lattice magnets (MnSi) are considered with (dirty sample) and without (clean sample) impurities. The dynamics of the magnetic structures in the two types of samples are analyzed by solving the LLG equation, including STT (adiabatic and non-adiabatic), and the impurities of the dirty material are added in the form of an effective field. This effective field is obtained from the Hamiltonian, which includes randomly distributed anisotropy defects with low concentration (0.1% impurity concentration) and easy axis normal to the sample plane. For these kinds of chiral materials, three magnetic structures can appear depending on the applied magnetic field (normal to the plane sample), a helical spin order for low applied field, a ferromagnetic phase for large applied field, and a triangular skyrmion crystal for intermediate fields. In Ref. 5, only the helical phase, for zero applied field, and the skyrmionic phase, when the field increases, are examined. The helical texture can be regarded as successively arranged ferromagnetic Bloch walls, and their dynamics are well described as a single domain-wall motion. The dynamic analysis of these two spin configurations shows two important results. On the one hand, the critical-current densities in the helical structure are larger than in the skyrmion-crystal spin configuration, even being an order of magnitude greater in some cases. On the other hand, in contrast to the helical structure, there exists a universal current–velocity relation of skyrmion motion, independent of the Gilbert damping, non-adiabatic effect, and impurities. The explanation of this behavior lies in the peculiar motion of skyrmions characterized by a flexible shape-deformation, to avoid pinning centers, of both individual skyrmions and the triangular lattice. The same authors found in Ref. 56 that in the skyrmion motion on a confined (with boundaries) disordered sample, the current–velocity relation does depend on the Gilbert damping, non-adiabatic effect, and impurities similar to that of ferromagnetic domain walls.

In the case of Ref. 92, the same disordered material as Ref. 5 is studied. Here, the random-distributed impurity concentration is larger (5%) and the dynamics of the skyrmion crystal is analyzed by numerically solving the LLG equation with STT for different anisotropy defect strengths, spin-polarized current densities, and applied magnetic fields. In this case, as the averaged impurity–impurity distance is much smaller than the skyrmion size, defects can be considered as grain defects and not point defects for the skyrmion dynamics. In the strongly disordered case (large anisotropy constant), four distinct phases appear as the current density increases: pinned state, depinned state, skyrmion multiplication/annihilation, and segregation of skyrmions. In contrast, in the weak disorder case, only the pinned and the depinned phases are present.

2. Set of effective potentials

When the rigid model is assumed, the disorder is incorporated by means of many effective potentials, which are added to Thiele's equation. These effective potentials can be of many types. An example is the case of potentials that simulate vacancies, such as in the work of Müller and Rosch,[55] which in addition to study a single hole defect, as was already discussed in Sec. III, the effect of weak disorder is also examined. This disorder is simulated as many vacancies, randomly distributed, with distances between defects much larger than the skyrmion radius. When the motion of a skyrmion is investigated in a disordered sample, the conclusions are that these kinds of defects can effectively accelerate the motion of the skyrmion and introduce an effective angle in its trajectory, respect to the one in a defect-free sample.

Other examples where the disorder is incorporated into the Thiele approximation are the works of Refs. 5 and 92. In addition to include anisotropy defects, as has just been seen in Sec. IV A 1, the intrinsic impurities are added in the Thiele equation as a phenomenological pinning force.[108,109] This phenomenological force is oriented opposite to the drift velocity, and its strength depends on both the number (and nature) of defects responsible for pinning and the elastic properties of the skyrmion lattice. The results show that when there is a weak disorder, although there is deformation on the individual skyrmion shape and its triangular lattice during the motion to avoid the impurities, Thiele's approximation remains valid as long as the discussed quantities (such as velocities and deviation angle) are averaged over space and time. However, the strongly disordered case cannot reproduce the numerical results obtained by solving the LLG equation because of the large skyrmion deformation.

As was already stated in Sec. III B 2, a Gaussian shape is an adequate function to simulate the effective potential of a single point defect. Therefore, another way to include disorder in a material is by incorporating many of these Gaussian defects. In Fig. 9, we can see examples of how a skyrmion can be trapped or scattered in a disordered sample, in this case with an average of 0.0028 randomly distributed Gaussian defects per unit of nm^2 (0.2 defect/l_{ex}^2), depending on the driving velocity.

In addition to the above three types, there is another way to include defects in the form of effective potentials to emulate disorder. In this case, the defect-skyrmion interaction is modeled as non-overlapping harmonic traps of size much smaller than the skyrmion size. The particle-based model of Ref. 71 (already discussed in Sec. III) is used, which is a version of Thiele's equation [with the Magnus-dissipation term, first term of Eq. (13)] that, in addition to the above defect-skyrmion interaction, also takes into account a skyrmion–skyrmion interaction and a driving force. The mutual interaction between skyrmions is simulated as a modified Bessel function of the relative distance between skyrmions and falls off exponentially for large skyrmion separations. The driving force represents a Lorentz force from an externally applied current.[52] In general, the damping term aligns the skyrmion velocity with the net force (driving, skyrmion–skyrmion, skyrmion-defect, and other forces) acting on the skyrmion, while the Magnus term partially rotates the velocity in the perpendicular direction.

In the literature, one can find many works that analyze the disorder in this way. Here, we show some examples of them.

Reichhardt *et al.*[93] studied collective skyrmion behaviors in random disordered samples (MnSi). The motion of a skyrmion lattice is characterized by the deviation angle introduced by the Magnus term, which is defined as $\theta = \arctan\left(\frac{\langle V_\perp \rangle}{\langle V_\parallel \rangle}\right)$, $\langle V_\perp \rangle \left(\langle V_\parallel \rangle\right)$ being the average skyrmion velocity in the direction perpendicular (parallel) to the applied drive. Reference 93 shows that the deviation angle is smaller in the cases of strong pinning or weak driving than in the case without disorder (clean sample). In addition, when the Magnus term dominates the depinning, the current density

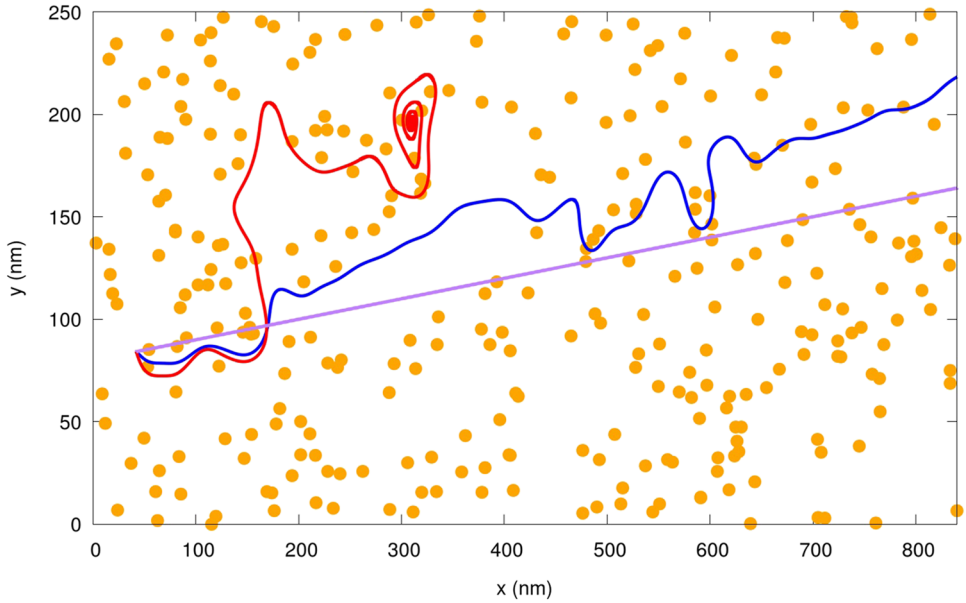

FIG. 9. Thiele's trajectories of a skyrmion driven by SHE in a disordered ferromagnet for the driving velocities ($\mathbb{N}\lambda_0\mathbf{v}_H/M_S^2$) of 260 m/s (in red) and 780 m/s (in blue). The disorder is taken into account by incorporating 400 attractive Gaussian potentials randomly distributed (orange dots) with $f_0 = 0.7$ (normalized to $M_S^2 Z\lambda_0$) and $\lambda_0 = 21$ nm. The average density of defects is 0.0028 defects/nm^2. For comparison, the trajectory of a driven skyrmion in a clean (without defects) sample is also plotted in purple. It is considered that $\mathbb{G}/M_S^3 Z = \mathbb{D}/M_S^2 Z = 4\pi$ and $\alpha = 0.3$.

threshold is reduced and spiraling trajectories are induced in the skyrmion motion due to the interaction with the pinning sites. The collective skyrmion–skyrmion interactions also contribute to the reduction of the depinning threshold. The different motion and pinned phases, as well as the transitions among them, are presented as a function of the driving strength, skyrmion density, and ratio between Magnus and damping terms.

In Ref. 94, the same authors carried out a similar study but emphasizing the behavior of the ratio between velocities $\frac{\langle V_\perp \rangle}{\langle V_\parallel \rangle}$ as a function of the driving force. Different defect densities and Magnus-damping ratios are considered. In general, the ratio between velocity components increases linearly with the drive strength before saturating at the value obtained without disorder. In the linear region, the slope increases when the Magnus contribution increases or the pinning strength decreases. For low defect densities, a nonlinear drive dependence is observed with a very abrupt initial growth.

Similar works analyze different aspects of the individual and collective dynamics of skyrmion in materials with periodic[95,96] and random disorder.[97–100] In Ref. 95, the dynamics of a skyrmion moving over a periodic pinning substrate is studied. The substrate force is applied by placing fixed skyrmions in a square lattice, and these skyrmions interact repulsively with a mobile skyrmion. The results of Ref. 95 show that the direction of motion of the skyrmion (deviation angle) is dependent on the amplitude of the external drive, only approaching the substrate-free limit for larger drives. The underlying symmetry of the substrate provides that skyrmion motion does not change continuously as a function of drive but rather forms a series of discrete steps related with the ratios of the velocity components perpendicular and parallel to the external drive direction. In each step, the deviation angle remains constant and the skyrmion moves in an orderly fashion throughout the sample. The number of steps in the transport curve increases when the relative strength of the Magnus term is increased. In addition, the skyrmion–substrate interactions can also produce an acceleration effect where the skyrmion velocity exceeds the value expected to be produced by the external drive.

Among the works of random disorder, Díaz *et al.*[97] examined distinct dynamical phases (plastic flow, moving liquid, moving smectic, and moving crystal phases) and transitions between these phases for varied intrinsic skyrmion deviation angles (Magnus and damping ratio) and drives. Reichhardt and Reichhardt[98] also presented a detailed study of the skyrmion transport, structure, and dynamics but varying the pinning strength, the skyrmion number to pinning sites ratio, and the Magnus force to the damping term ratio. This same work found a density segregation or skyrmion clustering effect that occurs for strong pinning and strong Magnus force. That is, the skyrmions form dense bands aligned with the driving direction that are separated by low density regions. A similar segregated behavior is also observed when skyrmions are driven over periodic arrays of parabolic pinning sites.[96]

In the cases of Díaz *et al.*[99] and Brown *et al.*,[100] the particle-based model is also used but without considering any externally applied current. On the one hand, in Ref. 99, the skyrmions are driven by their own interaction. The studied system consists of a pin-free region close to a pinned one with randomly placed nonoverlapping harmonic traps. The skyrmions are driven by a

gradient, introduced by slowly dropping skyrmions into the pin-free region and allowing them to move into the pinned region under the force of their mutual repulsion. Once the system reaches a steady state, individual skyrmions are added at a slow rate and the skyrmion avalanches are examined by measuring the average skyrmion velocity. The rate is slow enough to show well-defined avalanches separated by non-motion intervals. These avalanches are analyzed for different Magnus forces. In the case of small Magnus effect, the skyrmion avalanches exhibit power-law distributions in their duration and size, and the average avalanche shape for different avalanche duration can be scaled to a universal function. In contrast, when the ratio of the Magnus term to the damping term increases, a change in the universality class of the behavior occurs, the average avalanche shape becomes increasingly asymmetric, and individual avalanches exhibit motion in the direction perpendicular to their own density gradient.

On the other hand, Ref. 100 investigates the effects of quenched disorder on the relaxation dynamics of many mutually interacting skyrmions. The simulations are realized considering the particle-based model with random disorder and a thermal white noise. The time-dependent length used in the relaxation is the typical diffusion length. The results of Ref. 100 show that the attractive random disorder has a major effect on the relaxation processes because it limits the mobility of the skyrmions even to the point of introducing strong caging effect for low noise levels. The Magnus force, by adding a velocity component in the direction perpendicular to the propagation direction, allows skyrmions to route around obstacles and pinning centers rendering far more robust dynamics against pinning effects overall. Although in the absence of noise the Magnus force allows skyrmions to find pinning sites quicker (compared to systems without the Magnus force), when the noise strength increases, the fraction of pinned skyrmions decreases.

B. Granular sample with different grain properties

The second way to introduce disorder in the ferromagnetic material is to consider the whole sample as a set of different grains (see Fig. 10). To obtain the grain structure in the ferromagnet, a Voronoi tessellation is implemented.[110,111] The grains are generated from a set of randomly distributed points, known as Voronoi centers. From each Voronoi center, the associated grain is built with all the sample points that have that center as the closest one.

Most theoretical works analyzing disorder caused by sample granularity consider granular anisotropy. That is, each grain has a local uniaxial anisotropy that is given by a Gaussian distribution centered on the mean value K_u with a relative standard deviation of δK_u. Among these theoretical studies, we find the work of Garcia-Sanchez *et al.*[101] In a circular dot of Pt/Co/AlOx with a diameter of 150 nm and a thickness of 0.6 nm, the effect of a weak disorder on the skyrmion gyration is examined by using MuMax3. In confined geometries such as ultrathin film circular dots, spin-transfer torques due to current flowing perpendicular to the film plane lead to skyrmion oscillations. Spatial variations in the material parameters due to the presence of defects could induce fluctuations in the gyration orbit. Micromagnetic simulations reveal that weak disorder, δK_u = 1% and mean grain sizes between 2 and 20 nm (skyrmion size is 20–30 nm), does not influence the main characteristics (frequency and orbit) of the steady-state gyration.

Juge *et al.*[102] also studied the granularity effect over skyrmions in confined geometries. They examined a Pt/Co/MgO circular nanodot of 630 nm in diameter. For average grain sizes between 10 and 100 nm and different anisotropies, 2.5% ≤ δK_u ≤ 10%, skyrmion sizes and shapes are analyzed as a function of the applied magnetic field (see Fig. 11). Micromagnetic calculations, by means of MuMax3, show that at low pinning strength, the skyrmion diameter is approximately constant with the grain size (160–175 nm), whereas it increases on average for larger pinning strength (175–210 nm). At weak disorders and high magnetic fields, the skyrmion presents circular symmetry, but when the field decreases its amplitude, the quasi-circular skyrmion very often expands into an irregularly shaped domain. In contrast, when the anisotropy disorder is strong, the skyrmion shape and size are fully determined by the grains and the anisotropy mapping, while the small external magnetic field has little influence on the final state. The comparison between simulations and experimental measures (direct observation of the internal spin structure with x-ray magnetic circular dichroism combined with photo-emission electron microscopy) reveals that the influence of the magnetic field in the shape and diameter of skyrmions in Pt/Co/MgO systems is well reproduced by considering grain structures with local anisotropy variations.

Kim and Yoo[103] and Gong *et al.*,[104] in turn, studied the current-driven skyrmion dynamics in non-confined disordered films. Although the two works consider different material parameters, a similar general tendency is observed. That is, the disorder strongly influences the direction of the skyrmion propagation. A transverse motion, with respect to the propagation direction in the disorder-free case, is boosted by the granular anisotropy effect. In the

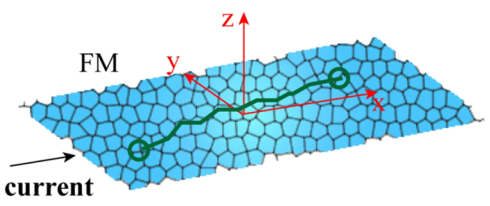

FIG. 10. Schematic illustration of a skyrmion in a granular chiral magnetic film [reproduced with permission from Gong *et al.*, Phys. Rev. B **101**, 064421 (2020). Copyright 2020, American Physical Society].

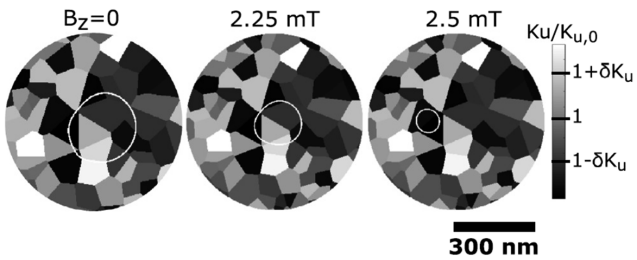

FIG. 11. Representation of the Néel domain walls delimiting the skyrmion ($|m_z| < 0.2$) on the grain structure for $B_z = 0$ (left), $B_z = 2.25$ mT (center), and $B_z = 2.5$ mT (right) with $m_z < 0$ inside the white border and $m_z > 0$ outside [reproduced with permission from Juge *et al.*, J. Magn. Magn. Mater. **455**, 3 (2018). Copyright 2018, Elsevier B. V.].

work of Ref. 103, MuMax3 micromagnetic calculations for different disorders (mean grain sizes between 10 and 20 nm and $5\% \leq \delta K_u \leq 10\%$) by taking into account STT or SHE are performed. The used parameters are consistent with the values of Pt/Co/AlOx multilayers. Simulation results reflect that, besides the obvious difference in spin torque efficiency, the behavior of the average skyrmion velocity as a function of the driven current density is similar for both torques. A pinning regime at low current density is exhibited, in which the average velocity is significantly below the value of the disorder-free case. As the current density increases, an exponential-like increase at low currents followed by a smooth transition toward the disorder-free case is observed. When the trajectory of a skyrmion is analyzed for low currents, it is observed that those few trajectories in which the skyrmion is not pinned exhibit an appreciable deflection angle with respect to the disorder-free case. This angle becomes less pronounced as the current is increased when the current-driven torques become sufficiently large to overcome the pinning potential. In addition, the skyrmion core fluctuates in size as it traverses the disorder potential especially at lower currents for which pinning is dominant.

Gong *et al.*, however, do not focus on analyzing the skyrmion deformations due to disorder but rather on explaining the origin of the transverse deviation in the skyrmion trajectories. The dynamics of the system is studied by solving the LLG equation with MuMax3 with adiabatic STT. The disorder is implemented with an average grain size (5 nm) comparable to the skyrmion size (7 nm) and $1\% \leq \delta K_u \leq 10\%$. Thiele simulations are also performed considering adiabatic STT with the disorder incorporated as a random force in all directions, obtained from the instantaneous micromagnetic energy of the skyrmion, and compared to the micromagnetic results. Matrix $\mathbb{D}$ is also recalculated at each time from the micromagnetic skyrmion structure. The results of both methods reveal that, in the skyrmion motion, three phases can be identified depending on the damping constant. One is the pinning phase when the disorder strength is above a critical value that depends on the driving current density. The second one is, below this critical disorder strength, the skyrmion transverse motion is boosted by the disorder below a critical damping, while the transverse motion is hindered above a critical damping. The critical damping depends on the current density and the disorder strength. In addition, it is also noted that when the random force is opposite to the driving force, the skyrmion transverse speed increases, while the longitudinal speed decreases. Finally, on the contrary, when the random force is along the driving force, the transverse speed decreases and the longitudinal speed increases.

The work of Saha *et al.*[105] is both an experimental and a theoretical study. This is an example of how to use the anisotropy granularity to simulate realistic systems and mimic the polycrystalline nature of the sample in order to properly compare experimental and simulated results. In this case, the skyrmion images in a Pt/Co/Ta sample are obtained with scanning transmission x-ray microscopy combined with x-ray magnetic circular dichroism, and they are compared with the numerical results obtained with MuMax3 with $\delta K_u = 10\%$. The aim of the work is to examine what is the adequate antidot (hole) lattice to improve the nucleation and confinement of skyrmions, and the experimental results validate the predictions obtained with micromagnetic simulations.

The work of Salimath *et al.*[106] is slightly different from those presented above. In this case, the anisotropy disorder is modeled as grains with uniform magnetic anisotropy strength and varying anisotropy direction. The anisotropy axis assigned to each grain is picked randomly within a conical region symmetric about the z axis (normal to the ferromagnetic thin sample) with a semiangle defined by φ. The current-driven motion of skyrmions in granular systems is studied using both micromagnetic modeling and Thiele's formalism. In the micromagnetic case, the LLG equation with STT is solved with OOMMF by considering parameters corresponding to Co/Pt systems. The disorder is simulated with average grain sizes between 7 and 100 nm and disorder strengths $2^\circ \leq \varphi \leq 5^\circ$. By considering that the relaxed skyrmion size is 18 nm, grain sizes above and below the skyrmion size are analyzed. Regarding the pinning and motion of the skyrmion, the results of Ref. 106 are equivalent to the ones presented in Refs. 103 and 104. On the one hand, depending on the grain size and the disorder strength, a significant pinning is observed. The disorder suppresses the longitudinal velocity component, with respect to the skyrmion driving direction in the clean (without defects) case, and gives rise to a threshold driving current density, whose value depends on the grain size, the defect density, and the disorder strength. This critical driving current reaches a maximum when the grain size is comparable to the skyrmion size. On the other hand, a skyrmion deviation in the transverse direction (with respect to the clean case) is also observed in

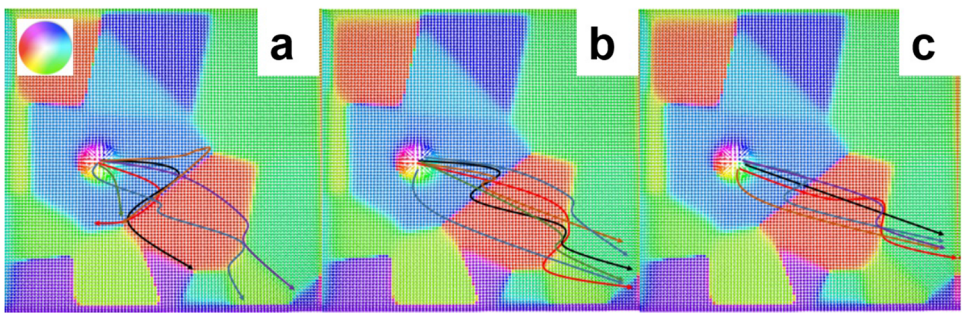

FIG. 12. Skyrmion trajectories in a polycrystalline sample with average grain size 57 nm and disorder strength $\varphi = 5^\circ$ for several realizations of anisotropy axis direction with increasing driving current densities from (a) to (c). The color scale represents the azimuthal angle of the magnetic moment. Reproduced with permission from Salimath *et al.*, Phys. Rev. B **99**, 104416 (2019). Copyright 2019, American Physics Society.

the presence of grains. This deviation is prominent in the case of small grains (compared with the skyrmion size), but for large grains and/or when the driving current density is increased, this effect is reduced. In addition to all this, it is also observed that when the grain size is much larger than the skyrmion size, the skyrmion motion is determined by the grain boundaries (see Fig. 12). At low current densities, the skyrmion exhibits a sliding motion along the boundary because the driving force is insufficient to overcome the repulsive potential formed by the grain boundaries. This motion channels the skyrmion toward the grain junction where it gets pinned. For intermediate current densities, the skyrmion can overcome the first grain boundary, but it slides on the second grain boundary before being depinned. By further increasing the current density, the skyrmion exhibits a reduced sliding motion because it becomes less sensitive to the grain boundaries. As a result, when the current density increases, the overall skyrmion trajectory straightens, reducing the overall transverse deviation. Equivalent results are obtained when the effects of the grain boundaries are examined by solving the Thiele equation with STT. The grain boundary is implemented in the equation as a quasi-one-dimensional repulsive Gaussian pinning potential of the form $\phi_{pin}(x,y) = \phi_0 \exp\left[-\frac{(x \sin\theta_b - y \cos\theta_b)^2}{R^2}\right]$, where ϕ_0 is the strength of the interaction, θ_b is the angle of the boundary, and R determines the interaction range.

Finally, we find the work of Legrand *et al.*[107] This is another example of experimental and theoretical work that includes granularity in its simulated samples in order to make them more realistic and to qualitatively understand the experimentally observed skyrmion motion. The simulations of the current-induced motion of multiple skyrmions in films are performed using MuMax3 with SHE. The chosen magnetic parameters are compatible with Ir/Co/Pt multilayers. The magnetic configuration is relaxed from a random magnetization distribution to obtain a population of skyrmions with a mean size of 24 nm. In the main text of Ref. 107, the granularity is simulated as local variations of the DM constant D. That is, each grain has a local DM constant, which is a Gaussian distribution centered at D with a relative standard deviation δD. However, in the supplementary material of the same work, other types of granular disorders are studied. The skyrmion motion is also studied by considering local variations of the exchange constant A, the saturation magnetization M_S, or the uniaxial anisotropy K_u. In the case of D inhomogeneities, the average grain size varies between 5 and 60 nm and the strength $\delta D = 10\%$ (see Fig. 13). In the case of the other kinds of grains, the mean grain size is 30 nm with defect strengths that vary between $5\% \le \delta A \le 10\%$, $1\% \le \delta K_u \le 10\%$, or $1\% \le \delta M_S \le 10\%$. By comparing inhomogeneities of the same relative amplitude, it appears that one can sort them, from higher to lower effect depending on the variable that varies: M_S, K_u, A, and D. The variations of any magnetic parameter affect the motion in the same way and are similar to the above granular works. That is, the greatest effects on skyrmion dynamics occur when skyrmion and grain sizes are similar and when the driving current density is small. These effects caused by inhomogeneities are basically three. First, the critical depinning current density is increased. The skyrmions are pinned, and its total distance traveled is reduced. Second, the skyrmion velocity is drastically reduced. Finally, a stronger deviation of the skyrmion trajectory, compared with the case without granularity, is observed. The magnetic disorder affects the gyrotropic motion of the skyrmions and causes their trajectories to align with the current direction reducing the deviation angle. All these theoretical results are in agreement with the experiments of the same work.

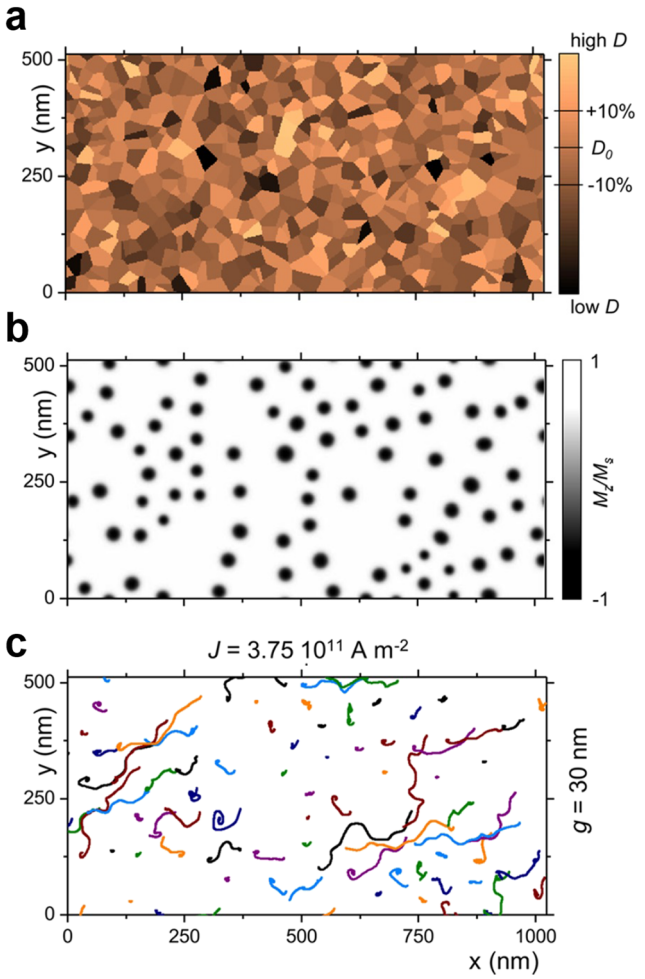

FIG. 13. (a) Map of the DM interaction in the simulation grid of 1024 × 512 nm^2, where the values are indicated by the color scale on the right, for grains with a size of 30 nm. (b) Initial state of the simulation after relaxing the skyrmion state showing M_z/M_S on a scale ranging from −1 (black) to 1 (white). (c) Trajectories of around 80 different skyrmions simulated with $J = 3.75 \cdot 10^{11}$ A m^{-2} [reproduced with permission from Legrand *et al.*, Nano Lett. **17**, 2703 (2017). Copyright 2017, American Chemical Society].

V. FINAL REMARKS

There are many ways to simulate defects in skyrmionic ferromagnetic materials depending on the nature, size, effect range, or number of defects. In this Research Update, we have presented a large sample of the most representative and relevant approaches to simulate defects. To end this paper and as a summary, we show Tables I–III. Due to the large amount of information and for ease of understanding, we have split the content into three tables. In

TABLE I. Summary (first part).

Type of defect	Process/Method	Theoretical basis	Study	Material	Reference
Substitution of atoms	Substitution of Mn (Si) by Zn, Ir, and Co (Pb)	DFT –> EHH	LDOS and pinning energies, values for MuMag constants	MnSi	22
Addition of atoms	Add transition metals 3d and 4d, Cu, Ag atoms	DFT –> EHH	LDOS and pinning energies	PdFe/Ir(111)	23
	Add clusters (dimers, trimers, and tetramers) of Cr and Fe atoms		Attraction/repulsion energies and values for MuMag constants		24
Local modification of EHH constants	Estimate minimum energy paths for transitions pinned-unpinned	EHH –> GNEB	Pinning energies, pinning positions and effective pinning potentials (for Thiele)	Co/Pt(111)	25
	Find extra terms in EHH due to defects	EHH –> analytic	Effective fields (for LLG) and effective potentials (for thiele)	Generic	26
Vacancies	Remove magnetic moments of atoms	EHH –> GNEB	Annihilation/nucleation and pinning/depinning processes	PdFe	27
			Pinning energies and positions, and effective potentials	Co/Pt(111)	25
Holes (zero magnetization regions)	Drive skyrmion with STT and find trajectories	LLG + STT	Possibility of pinning	Generic	55
			Nucleation of skyrmions at border notches	MnSi	56
			Compare energy barriers for annihilating skyrmions and overcoming pinning sites	Pt/Co/Ta	57
Local modulation of thickness	Establish a phase diagram of minimum-energy magnetic state vs applied field and thickness film	LLG	Control of pinning sites	FeGe	61
Local curvature of sample	Find effective interactions due to curvature	Micromagnetic energy	Pinning positions	Generic	62
		Micromagnetic energy and LLG + STT	Trajectories and pinning positions	FeGe	63
Gaussian-like position-dependence of micromagnetic constants	Fit different defect effects with STM experiments	Micromagnetic energy	Interaction energies skyrmion-defect (energy vs distance)	PdFe/Ir(111)	69
	Find trajectories changing model parameters	LLG	Skyrmion dynamics around defects	Generic	70

TABLE II. Summary (second part).

Type of defect	Process/Method	Theoretical basis	Study	Material	Reference
Exponential-like position-dependence of exchange constant	Find skyrmion energies by changing defect parameters	Micromagnetic energy	Interaction energies skyrmion-defect (energy vs distance) to obtain the defect effective force (for Thiele)	MnSi	71
Regions with different micromagnetic constants	Change the defect size and/or type	LLG	Trapping or repulsion of skyrmion	Co/Pt	73
		LLG + OOPT	Driving current–density dependence		16
			Interaction with two skyrmions		74
Change in anisotropy (value and/or direction)	Apply a DC current and evaluate evolution	LLG + STT	Periodical nucleation of skyrmion	CoCrPt/Ti	77
Change in DM constant	Find trajectories with different parameters	LLG + STT	Confinement of skyrmions in prepatterned regions	Co/Pt multilayers	80
			Acceleration, guiding of skyrmion along defects		60
Hole as effective potential	Find trajectories with different potential models	Thiele + STT	Capturing of skyrmion	Generic	55
Gaussian-like effective potential	Solve Thiele's equation with different parameters	Thiele and Thiele + STT	Spiraling trajectories around defects	Generic	70
		Thiele + SHE			49
Gaussian-like effective potential with temperature	Solve FPE at different temperatures	Thiele –> FPE	Probability density of trapping/escaping skyrmion	Generic	87
Extended linear defects with effective potential	Find the effective potential for extended defects and solve Thiele's equation	Thiele + SHE	Analytical expression for the L-shaped, grid, . . . defects	Generic and Co/Pt multilayers	49
Extended defects as sinusoidal or exponential effective potentials	Solve Thiele's equation for different parameters	Thiele + STT	Relative importance of the magnus/pinning forces	Generic	91
Many anisotropy defects randomly distributed	Compare the driving current needed to move skyrmions in clean and dirty samples	LLG + STT	Universal driving current-skyrmions velocity relation	MnSi	5
	Evaluate the skyrmions dynamics for different defect strengths, driving currents, and applied fields.		Obtaining different phases of skyrmion crystal: Pinned, depinned, multiplication, and segregation		92

TABLE III. Summary (third part).

Type of defect	Process/Method	Theoretical basis	Study	Material	References
Many defects randomly distributed –> phenomenological pinning force	Solve Thiele's equation with a phenomenological pinning force opposite to the drift velocity	Thiele + STT	Validity of Thiele approximation outputs (averaged velocities and deviation angles) when the disorder is low	MnSi	5 and 92
Many defects randomly distributed as effective potentials	Solving particle-based model (71), including skyrmion–skyrmion interaction, in several conditions		Find averaged skyrmions dynamics (velocity, hall angle, . . .)		93 and 94
			Different dynamical phases: Plastic flow, moving liquid, moving smectic, and moving crystal phases		97
			Segregation, clustering		98
		Thiele	Avalanches		99
	Solving particle-based model, including skyrmion–skyrmion interaction and thermal noise		Quenched disorder, diffusion		100
Many defects periodically distributed as effective potentials	Solving particle-based model, including skyrmion–skyrmion interaction	Thiele + STT	Skyrmion dynamics (velocity, sky hall angle, . . .) and dependence on the underlying potential, segregation		95 and 96
Granularity by anisotropy variation with Voronoi grains (Voronoi tessellation) in confined geometries	Confinement properties and study of the oscillations in perpendicular driving current	LLG + OOPT	Influence on the steady-state gyration	Pt/Co/AlOx	101
	Variation of granular properties modeling	LLG	Size and shape of skyrmions, comparison with experiments	Pt/Co/MgO	102
	Use the adequate parameters in the simulation of granular sample after comparison with the experiments		Adequate antidot lattice to improve skyrmion nucleation in a disordered (polycrystalline) sample	Pt/Co/Ta	105
Granularity by anisotropy variation with Voronoi grains in non-confined geometries	Variation of granular properties modeling	LLG + STT or SHE	Skyrmion propagation and deformation	Pt/Co systems	103
		LLG + STT and Thiele	Transverse deviation in skyrmion trajectories		104
			Skyrmion trajectories in large grains. Effects of boundaries		106
Granularity by DM variation (among others) with Voronoi grains	Variation of granular properties modeling	LLG + SHE	Skyrmion trajectories. Effects of grain size	Ir/Co/Pt	107

Tables I–III, we find the simulated defect type, the process or method followed to make the simulation, and the theoretical framework that encompasses it. We also insert a brief description of the study carried out, the material compatible with the parameters used, and the reference where one can find all the information.

ACKNOWLEDGMENTS

We acknowledge financial support from Catalan project 2017-SGR-105 and Spanish project PID2019-104670GB-I00 of the Agencia Estatal de Investigación/Fondo Europeo de Desarrollo Regional (UE). J.C.-Q. acknowledges a grant (Grant No. FPU17/01970) from the Ministerio de Ciencia, Innovación y Universidades (Spanish Government).

AUTHOR DECLARATIONS

Conflict of Interest

We have no conflicts of interest to disclose.

DATA AVAILABILITY

The data that support the findings of this study are available within the article.

REFERENCES

[1]S. Mühlbauer, B. Binz, F. Jonietz, C. Pfleiderer, A. Rosch, A. Neubauer, R. Georgii, and P. Böni, "Skyrmion lattice in a chiral magnet," Science **323**, 915 (2009).
[2]X. Z. Yu, Y. Onose, N. Kanazawa, J. H. Park, J. H. Han, Y. Matsui, N. Nagaosa, and Y. Tokura, "Real-space observation of a two-dimensional skyrmion crystal," Nature **465**, 901 (2010).
[3]F. Jonietz, S. Mühlbauer, C. Pfleiderer, A. Neubauer, W. Münzer, A. Bauer, T. Adams, R. Georgii, P. Böni, R. A. Duine, K. Everschor, M. Garst, and A. Rosch, "Spin transfer torques in MnSi at ultralow current densities," Science **330**, 1648 (2010).
[4]X. Z. Yu, N. Kanazawa, W. Z. Zhang, T. Nagai, T. Hara, K. Kimoto, Y. Matsui, Y. Onose, and Y. Tokura, "Skyrmion flow near room temperature in an ultralow current density," Nat. Commun. **3**, 988 (2012).
[5]J. Iwasaki, M. Mochizuki, and N. Nagaosa, "Universal current-velocity relation of skyrmion motion in chiral magnets," Nat. Commun. **4**, 1463 (2013).
[6]A. Fert, V. Cros, and J. Sampaio, "Skyrmions on the track," Nat. Nanotechnol. **8**, 152 (2013).
[7]N. Nagaosa and Y. Tokura, "Topological properties and dynamics of magnetic skyrmions," Nat. Nanotechnol. **8**, 899 (2013).
[8]J. P. Liu, Z. Zhang, and G. Zhao, *Skyrmions: Topological Structures, Properties, and Applications* (CRC Press, Taylor and Francis Group, 2016).
[9]N. Mathur, M. J. Stolt, and S. Jin, "Magnetic skyrmions in nanostructures of noncentrosymmetric materials," APL Mater. **7**, 120703 (2019).
[10]R. Wiesendanger, "Nanoscale magnetic skyrmions in metallic films and multilayers: A new twist for spintronics," Nat. Rev. Mater. **1**, 16044 (2016).
[11]A. Fert, N. Reyren, and V. Cros, "Magnetic skyrmions: Advances in physics and potential applications," Nat. Rev. Mater. **2**, 17031 (2017).
[12]K. Everschor-Sitte, J. Masell, R. M. Reeve, and M. Kläui, "Perspective: Magnetic skyrmions—Overview of recent progress in an active research field," J. Appl. Phys. **124**, 240901 (2018).
[13]C. Moreau-Luchaire, C. Moutafis, N. Reyren, J. Sampaio, C. A. Vaz, N. Van Horne, K. Bouzehouane, K. Garcia, C. Deranlot, P. Warnicke, P. Wohlhüter, J. M. George, M. Weigand, J. Raabe, V. Cros, and A. Fert, "Additive interfacial chiral interaction in multilayers for stabilization of small individual skyrmions at room temperature," Nat. Nanotechnol. **11**, 444 (2016).
[14]P. Ho, A. K. Tan, S. Goolaup, A. L. Oyarce, M. Raju, L. S. Huang, A. Soumyanarayanan, and C. Panagopoulos, "Geometrically tailored skyrmions at zero magnetic field in multilayered nanostructures," Phys. Rev. Appl. **11**, 024064 (2019).
[15]N. S. Kiselev, A. N. Bogdanov, R. Schäfer, and U. K. Röler, "Chiral skyrmions in thin magnetic films: New objects for magnetic storage technologies?," J. Phys. D: Appl. Phys. **44**, 392001 (2011).
[16]J. Sampaio, V. Cros, S. Rohart, A. Thiaville, and A. Fert, "Nucleation, stability and current-induced motion of isolated magnetic skyrmions in nanostructures," Nat. Nanotechnol. **8**, 839 (2013).
[17]H. Kronmüller and M. Fähnle, *Micromagnetism and the Microstructure of Ferromagnetic Solids* (Cambridge University Press, 2003).
[18]A. Aharoni, *Introduction to the Theory of Ferromagnetism*, 2nd ed. (Oxford University Press, 2000).
[19]K. J. Harte, "Theory of magnetization ripple in ferromagnetic films," J. Appl. Phys. **39**, 1503 (1968).
[20]S. Rohart, J. Miltat, and A. Thiaville, "Path to collapse for an isolated Néel skyrmion," Phys. Rev. B **93**, 214412 (2016).
[21]I. S. Lobanov, H. Jónsson, and V. M. Uzdin, "Mechanism and activation energy of magnetic skyrmion annihilation obtained from minimum energy path calculations," Phys. Rev. B **94**, 174418 (2016).
[22]H. C. Choi, S. Z. Lin, and J. X. Zhu, "Density functional theory study of skyrmion pinning by atomic defects in MnSi," Phys. Rev. B **93**, 115112 (2016).
[23]I. Lima Fernandes, J. Bouaziz, S. Blügel, and S. Lounis, "Universality of defect-skyrmion interaction profiles," Nat. Commun. **9**, 4395 (2018).
[24]I. Gede Arjana, I. Lima Fernandes, J. Chico, and S. Lounis, "Sub-nanoscale atom-by-atom crafting of skyrmion-defect interaction profiles," Sci. Rep. **10**, 14655 (2020).
[25]D. Stosic, T. B. Ludermir, and M. V. Milošević, "Pinning of magnetic skyrmions in a monolayer Co film on Pt(111): Theoretical characterization and exemplified utilization," Phys. Rev. B **96**, 214403 (2017).
[26]C. Navau, N. Del-Valle, and A. Sanchez, "Interaction of isolated skyrmions with point and linear defects," J. Magn. Magn. Mater. **465**, 709 (2018).
[27]M. Potkina, I. Lobanov, and V. Uzdin, "Nonmagnetic impurities in skyrmion racetrack memory," Nanosyst.: Phys., Chem., Math. **11**, 628 (2020).
[28]S. H. Vosko, L. Wilk, and M. Nusair, "Accurate spin-dependent electron liquid correlation energies for local spin density calculations: A critical analysis," Can. J. Phys. **58**, 1200 (1980).
[29]D. M. Crum, M. Bouhassoune, J. Bouaziz, B. Schweflinghaus, S. Blügel, and S. Lounis, "Perpendicular reading of single confined magnetic skyrmions," Nat. Commun. **6**, 8541 (2015).
[30]D. Joubert, "From ultrasoft pseudopotentials to the projector augmented-wave method," Phys. Rev. B **59**, 1758 (1999).
[31]N. Papanikolaou, R. Zeller, and P. H. Dederichs, "Conceptual improvements of the KKR method," J. Phys.: Condens. Matter **14**, 2799 (2002).
[32]D. S. G. Bauer, "Development of a relativistic full-potential first-principles multiple scattering Green function method applied to complex magnetic textures of nano structures at surfaces," Ph.D. thesis/dissertation, Zugl.: Aachen Technische Hochschule, Jülich, 2013, Druckausgabe: 2013, Onlineausgabe: 2014.
[33]P. F. Bessarab, V. M. Uzdin, and H. Jónsson, "Method for finding mechanism and activation energy of magnetic transitions, applied to skyrmion and antivortex annihilation," Comput. Phys. Commun. **196**, 335 (2015).
[34]A. A. Thiele, "Steady-state motion of magnetic domains," Phys. Rev. Lett. **30**, 230 (1973).
[35]J. Hagemeister, N. Romming, K. von Bergmann, E. Y. Vedmedenko, and R. Wiesendanger, "Stability of single skyrmionic bits," Nat. Commun. **6**, 8455 (2015).
[36]W. F. J. Brown, *Magnetostatic Principles in Ferromagnetism* (North-Holland Pub. Co., 1962).
[37]S. Zhang and Z. Li, "Roles of nonequilibrium conduction electrons on the magnetization dynamics of ferromagnets," Phys. Rev. Lett. **93**, 127204 (2004).
[38]A. N. Bogdanov and U. K. Rössler, "Chiral symmetry breaking in magnetic thin films and multilayers," Phys. Rev. Lett. **87**, 037203 (2001).
[39]J. M. D. Coey, *Magnetism and Magnetic Materials* (Cambridge University Press, 2010).

[40]S. Rohart, V. Repain, A. Thiaville, and S. Rousset, "Limits of the macrospin model in cobalt nanodots with enhanced edge magnetic anisotropy," Phys. Rev. B **76**, 104401 (2007).
[41]S. Rohart and A. Thiaville, "Skyrmion confinement in ultrathin film nanostructures in the presence of Dzyaloshinskii–Moriya interaction," Phys. Rev. B **88**, 184422 (2013).
[42]H. Yang, A. Thiaville, S. Rohart, A. Fert, and M. Chshiev, "Anatomy of Dzyaloshinskii–Moriya interaction at Co/Pt interfaces," Phys. Rev. Lett. **115**, 267210 (2015).
[43]S. Woo, K. Litzius, B. Krüger, M. Y. Im, L. Caretta, K. Richter, M. Mann, A. Krone, R. M. Reeve, M. Weigand, P. Agrawal, I. Lemesh, M. A. Mawass, P. Fischer, M. Kläui, and G. S. Beach, "Observation of room-temperature magnetic skyrmions and their current-driven dynamics in ultrathin metallic ferromagnets," Nat. Mater. **15**, 501 (2016).
[44]D. Mike and P. Don, The object oriented micromagnetic framework (OOMMF) project at ITL/NIST, https://math.nist.gov/oommf/.
[45]R. Stanislas and Z. Xichao, OOMMF package for Dzyaloshinsky–Moriya interaction, https://www.lps.u-psud.fr/spip.php?article2252&lang=fr.
[46]A. Vansteenkiste, J. Leliaert, M. Dvornik, M. Helsen, F. Garcia-Sanchez, and B. V. Waeyenberge, "The design and verification of MuMax3," AIP Adv. **4**, 107133 (2014).
[47]A. Vansteenkiste, "MuMax3 GPU-accelerated micromagnetism, https://mumax.github.io/.
[48]R. Tomasello, E. Martinez, R. Zivieri, L. Torres, M. Carpentieri, and G. Finocchio, "A strategy for the design of skyrmion racetrack memories," Sci. Rep. **4**, 6784 (2014).
[49]L. González-Gómez, J. Castell-Queralt, N. Del-Valle, A. Sanchez, and C. Navau, "Analytical modeling of the interaction between skyrmions and extended defects," Phys. Rev. B **100**, 054440 (2019).
[50]Z. Li and S. Zhang, "Domain-wall dynamics and spin-wave excitations with spin-transfer torques," Phys. Rev. Lett. **92**, 207203 (2004).
[51]Y. B. Bazaliy, B. Jones, and S. C. Zhang, "Modification of the Landau-Lifshitz equation in the presence of a spin-polarized current in colossal- and giant-magnetoresistive materials," Phys. Rev. B **57**, R3213 (1998).
[52]L. Liu, O. J. Lee, T. J. Gudmundsen, D. C. Ralph, and R. A. Buhrman, "Current-induced switching of perpendicularly magnetized magnetic layers using spin torque from the spin Hall effect," Phys. Rev. Lett. **109**, 096602 (2012).
[53]W. Jiang, X. Zhang, G. Yu, W. Zhang, X. Wang, M. B. Jungfleisch, J. E. Pearson, X. Cheng, O. Heinonen, K. L. Wang, Y. Zhou, A. Hoffmann, and S. G. T. Velthuis, "Direct observation of the skyrmion Hall effect," Nat. Phys. **13**, 162 (2017).
[54]A. V. Khvalkovskiy, V. Cros, D. Apalkov, V. Nikitin, M. Krounbi, K. A. Zvezdin, A. Anane, J. Grollier, and A. Fert, "Matching domain-wall configuration and spin-orbit torques for efficient domain-wall motion," Phys. Rev. B **87**, 020402 (2013).
[55]J. Müller and A. Rosch, "Capturing of a magnetic skyrmion with a hole," Phys. Rev. B **91**, 054410 (2015).
[56]J. Iwasaki, M. Mochizuki, and N. Nagaosa, "Current-induced skyrmion dynamics in constricted geometries," Nat. Nanotechnol. **8**, 742 (2013).
[57]D. Suess, C. Vogler, F. Bruckner, P. Heistracher, F. Slanovc, and C. Abert, "Spin torque efficiency and analytic error rate estimates of skyrmion racetrack memory," Sci. Rep. **9**, 4827 (2019).
[58]S. Luo, M. Song, X. Li, Y. Zhang, J. Hong, X. Yang, X. Zou, N. Xu, and L. You, "Reconfigurable skyrmion logic gates," Nano Lett. **18**, 1180 (2018).
[59]M. Chauwin, X. Hu, F. Garcia-Sanchez, N. Betrabet, A. Paler, C. Moutafis, and J. S. Friedman, "Skyrmion logic system for large-scale reversible computation," Phys. Rev. Appl. **12**, 064053 (2019).
[60]J. Castell-Queralt, L. González-Gómez, N. Del-Valle, A. Sanchez, and C. Navau, "Accelerating, guiding, and compressing skyrmions by defect rails," Nanoscale **11**, 12589 (2019).
[61]S. A. Pathak and R. Hertel, "Geometrically constrained skyrmions," Magnetochemistry **7**, 26 (2021).
[62]V. P. Kravchuk, D. D. Sheka, A. Kákay, O. M. Volkov, U. K. Rößler, J. van den Brink, D. Makarov, and Y. Gaididei, "Multiplet of skyrmion states on a curvilinear defect: Reconfigurable skyrmion lattices," Phys. Rev. Lett. **120**, 067201 (2018).
[63]V. L. Carvalho-Santos, M. A. Castro, D. Salazar-Aravena, D. Laroze, R. M. Corona, S. Allende, and D. Altbir, "Skyrmion propagation along curved racetracks," Appl. Phys. Lett. **118**, 172407 (2021).
[64]V. P. Kravchuk, U. K. Rößler, O. M. Volkov, D. D. Sheka, J. van den Brink, D. Makarov, H. Fuchs, H. Fangohr, and Y. Gaididei, "Topologically stable magnetization states on a spherical shell: Curvature-stabilized skyrmions," Phys. Rev. B **94**, 144402 (2016).
[65]R. Streubel, P. Fischer, F. Kronast, V. P. Kravchuk, D. D. Sheka, Y. Gaididei, O. G. Schmidt, and D. Makarov, "Magnetism in curved geometries," J. Phys. D: Appl. Phys. **49**, 363001 (2016).
[66]J. Yang, C. Abert, D. Suess, and S. K. Kim, "Intrinsic DMI-free skyrmion formation and robust dynamic behaviors in magnetic hemispherical shells," Sci. Rep. **11**, 3886 (2021).
[67]D. D. Sheka, O. V. Pylypovskyi, P. Landeros, Y. Gaididei, A. Kákay, and D. Makarov, "Nonlocal chiral symmetry breaking in curvilinear magnetic shells," Commun. Phys. **3**, 128 (2020).
[68]Y. Gaididei, V. P. Kravchuk, and D. D. Sheka, "Curvature effects in thin magnetic shells," Phys. Rev. Lett. **112**, 257203 (2014).
[69]C. Hanneken, A. Kubetzka, K. V. Bergmann, and R. Wiesendanger, "Pinning and movement of individual nanoscale magnetic skyrmions via defects," New J. Phys. **18**, 055009 (2016).
[70]Y. H. Liu and Y. Q. Li, "A mechanism to pin skyrmions in chiral magnets," J. Phys.: Condens. Matter **25**, 076005 (2013).
[71]S. Z. Lin, C. Reichhardt, C. D. Batista, and A. Saxena, "Particle model for skyrmions in metallic chiral magnets: Dynamics, pinning, and creep," Phys. Rev. B **87**, 214419 (2013).
[72]J. Zang, M. Mostovoy, J. H. Han, and N. Nagaosa, "Dynamics of skyrmion crystals in metallic thin films," Phys. Rev. Lett. **107**, 136804 (2011).
[73]D. Toscano, S. A. Leonel, P. Z. Coura, and F. Sato, "Building traps for skyrmions by the incorporation of magnetic defects into nanomagnets: Pinning and scattering traps by magnetic properties engineering," J. Magn. Magn. Mater. **480**, 171 (2019).
[74]J. Ding, X. Yang, and T. Zhu, "Manipulating current induced motion of magnetic skyrmions in the magnetic nanotrack," J. Phys. D: Appl. Phys. **48**, 115004 (2015).
[75]P. J. Metaxas, J. P. Jamet, A. Mougin, M. Cormier, J. Ferré, V. Baltz, B. Rodmacq, B. Dieny, and R. L. Stamps, "Creep and flow regimes of magnetic domain-wall motion in ultrathin Pt/Co/Pt films with perpendicular anisotropy," Phys. Rev. Lett. **99**, 217208 (2007).
[76]C. Chappert, H. Bernas, J. Ferré, V. Kottler, J. Jamet, Y. Chen, E. Cambril, T. Devolder, F. Rousseaux, V. Mathet, and H. Launois, "Planar patterned magnetic media obtained by ion irradiation," Science **280**, 1919 (1998).
[77]K. Everschor-Sitte, M. Sitte, T. Valet, A. Abanov, and J. Sinova, "Skyrmion production on demand by homogeneous DC currents," New J. Phys. **19**, 092001 (2017).
[78]Y. F. Zheng, J. P. Wang, and V. Ng, "Control of the tilted orientation of CoCrPt/Ti thin film media by collimated sputtering," J. Appl. Phys. **91**, 8007 (2002).
[79]A. Drews, G. Selke, B. Krueger, C. Abert, and T. Gerhardt, Micromagnum, http://micromagnetics.org/magnum.fd/index.html#.
[80]J. Mulkers, B. V. Waeyenberge, and M. V. Milošević, "Effects of spatially engineered Dzyaloshinskii-Moriya interaction in ferromagnetic films," Phys. Rev. B **95**, 144401 (2017).
[81]A. Hrabec, N. A. Porter, A. Wells, M. J. Benitez, G. Burnell, S. McVitie, D. McGrouther, T. A. Moore, and C. H. Marrows, "Measuring and tailoring the Dzyaloshinskii-Moriya interaction in perpendicularly magnetized thin films," Phys. Rev. B **90**, 020402 (2014).
[82]J. Cho, N. H. Kim, S. Lee, J. S. Kim, R. Lavrijsen, A. Solignac, Y. Yin, D. S. Han, N. J. van Hoof, H. J. Swagten, B. Koopmans, and C. Y. You, "Thickness dependence of the interfacial Dzyaloshinskii–Moriya interaction in inversion symmetry broken systems," Nat. Commun. **6**, 7635 (2015).
[83]N. H. Kim, D. S. Han, J. Jung, J. Cho, J. S. Kim, H. J. Swagten, and C. Y. You, "Improvement of the interfacial Dzyaloshinskii-Moriya interaction by introducing a Ta buffer layer," Appl. Phys. Lett. **107**, 142408 (2015).
[84]J. Iwasaki, W. Koshibae, and N. Nagaosa, "Colossal spin transfer torque effect on skyrmion along the edge," Nano Lett. **14**, 4432 (2014).

[85]X. Zhang, G. P. Zhao, H. Fangohr, J. P. Liu, W. X. Xia, J. Xia, and F. J. Morvan, "Skyrmion-skyrmion and skyrmion-edge repulsions in skyrmion-based racetrack memory," Sci. Rep. **5**, 7643 (2015).
[86]C. Navau, N. Del-Valle, and A. Sanchez, "Analytical trajectories of skyrmions in confined geometries: Skyrmionic racetracks and nano-oscillators," Phys. Rev. B **94**, 184104 (2016).
[87]J. Castell-Queralt, L. González-Gómez, N. Del-Valle, and C. Navau, "Deterministic approach to skyrmionic dynamics at nonzero temperatures: Pinning sites and racetracks," Phys. Rev. B **101**, 140404 (2020).
[88]X. Zhang, M. Ezawa, and Y. Zhou, "Thermally stable magnetic skyrmions in multilayer synthetic antiferromagnetic racetracks," Phys. Rev. B **94**, 064406 (2016).
[89]J. Miltat, S. Rohart, and A. Thiaville, "Brownian motion of magnetic domain walls and skyrmions, and their diffusion constants," Phys. Rev. B **97**, 214426 (2018).
[90]H. Risken and T. Frank, *The Fokker-Planck Equation: Methods of Solutions and Applications*, Springer Series in Synergetics (Springer, 1996).
[91]J. C. Martinez and M. B. A. Jalil, "Topological dynamics and current-induced motion in a skyrmion lattice," New J. Phys. **18**, 033008 (2016).
[92]W. Koshibae and N. Nagaosa, "Theory of current-driven skyrmions in disordered magnets," Sci. Rep. **8**, 6328 (2018).
[93]C. Reichhardt, D. Ray, and C. J. Reichhardt, "Collective transport properties of driven skyrmions with random disorder," Phys. Rev. Lett. **114**, 217202 (2015).
[94]C. Reichhardt and C. J. O. Reichhardt, "Noise fluctuations and drive dependence of the skyrmion Hall effect in disordered systems," New J. Phys. **18**, 095005 (2016).
[95]C. Reichhardt, D. Ray, and C. J. Reichhardt, "Quantized transport for a skyrmion moving on a two-dimensional periodic substrate," Phys. Rev. B **91**, 104426 (2015).
[96]C. Reichhardt, D. Ray, and C. J. Reichhardt, "Nonequilibrium phases and segregation for skyrmions on periodic pinning arrays," Phys. Rev. B **98**, 134418 (2018).
[97]S. A. Díaz, C. J. Reichhardt, D. P. Arovas, A. Saxena, and C. Reichhardt, "Fluctuations and noise signatures of driven magnetic skyrmions," Phys. Rev. B **96**, 085106 (2017).
[98]C. Reichhardt and C. J. Reichhardt, "Nonlinear transport, dynamic ordering, and clustering for driven skyrmions on random pinning," Phys. Rev. B **99**, 104418 (2019).
[99]S. A. Díaz, C. Reichhardt, D. P. Arovas, A. Saxena, and C. J. O. Reichhardt, "Avalanches and criticality in driven magnetic skyrmions," Phys. Rev. Lett. **120**, 117203 (2018).
[100]B. L. Brown, U. C. Täuber, and M. Pleimling, "Skyrmion relaxation dynamics in the presence of quenched disorder," Phys. Rev. B **100**, 024410 (2019).
[101]F. Garcia-Sanchez, J. Sampaio, N. Reyren, V. Cros, and J. V. Kim, "A skyrmion-based spin-torque nano-oscillator," New J. Phys. **18**, 075011 (2016).
[102]R. Juge, S. G. Je, D. de Souza Chaves, S. Pizzini, L. D. Buda-Prejbeanu, L. Aballe, M. Foerster, A. Locatelli, T. O. Menteş, A. Sala, F. Maccherozzi, S. S. Dhesi, S. Auffret, E. Gautier, G. Gaudin, J. Vogel, and O. Boulle, "Magnetic skyrmions in confined geometries: Effect of the magnetic field and the disorder," J. Magn. Magn. Mater. **455**, 3 (2018).
[103]J. V. Kim and M. W. Yoo, "Current-driven skyrmion dynamics in disordered films," Appl. Phys. Lett. **110**, 132404 (2017).
[104]X. Gong, H. Y. Yuan, and X. R. Wang, "Current-driven skyrmion motion in granular films," Phys. Rev. B **101**, 064421 (2020).
[105]S. Saha, M. Zelent, S. Finizio, M. Mruczkiewicz, S. Tacchi, A. K. Suszka, S. Wintz, N. S. Bingham, J. Raabe, M. Krawczyk, and L. J. Heyderman, "Formation of Neél-type skyrmions in an antidot lattice with perpendicular magnetic anisotropy," Phys. Rev. B **100**, 144435 (2019).
[106]A. Salimath, A. Abbout, A. Brataas, and A. Manchon, "Current-driven skyrmion depinning in magnetic granular films," Phys. Rev. B **99**, 104416 (2019).
[107]W. Legrand, D. Maccariello, N. Reyren, K. Garcia, C. Moutafis, C. Moreau-Luchaire, S. Collin, K. Bouzehouane, V. Cros, and A. Fert, "Room-temperature current-induced generation and motion of sub-100 nm skyrmions," Nano Lett. **17**, 2703 (2017).
[108]K. Everschor, M. Garst, B. Binz, F. Jonietz, S. Mühlbauer, C. Pfleiderer, and A. Rosch, "Rotating skyrmion lattices by spin torques and field or temperature gradients," Phys. Rev. B **86**, 054432 (2012).
[109]T. Schulz, R. Ritz, A. Bauer, M. Halder, M. Wagner, C. Franz, C. Pfleiderer, K. Everschor, M. Garst, and A. Rosch, "Emergent electrodynamics of skyrmions in a chiral magnet," Nat. Phys. **8**, 301 (2012).
[110]J. W. Lau, R. D. Memichael, and M. J. Donahue, "Implementation of two-dimensional polycrystalline grains in object oriented micromagnetic framework," J. Res. Natl. Inst. Stand. Technol. **114**, 57 (2009).
[111]J. Leliaert, B. V. D. Wiele, A. Vansteenkiste, L. Laurson, G. Durin, L. Dupré, and B. V. Waeyenberge, "Current-driven domain wall mobility in polycrystalline Permalloy nanowires: A numerical study," J. Appl. Phys. **115**, 233903 (2014).